TAMPEREEN TEKNILLINEN YLIOPISTO
TAMPERE UNIVERSITY OF TECHNOLOGY

TAEHOON KIM

FORCE FEEDBACK CONTROL IN MATERIAL TESTING APPLICATIONS

Master of Science thesis

Examiner: prof. Pasi Kallio
Examiner and topic approved by the Faculty Council of the Faculty of Engineering Sciences
on 5th October 2016

ABSTRACT

TAEHOON KIM
Tampere University of Technology
Master of Science Thesis, 69 pages
December 2017
Master's Degree Programme in Automation Engineering
Major: Mechatronics and Micromachines
Examiner: Professor Pasi Kallio

Keywords: Force control, Feedback control system, Micro-scale fibrous material testing, Microrobotic technology, Fibrous material, glass fiber, specimen handling.

In micro- and nano scale material testing applications, the force control has been significantly used for stable and accurate manipulation. This thesis introduces new application area of the force feedback control in the tensile testing of the micro-scale fibrous materials. Specifically, the force feedback controller is implemented in existing open loop microrobotic platform which simply consists of two clamps. One clamp is driven by a M.111.1 DG Micro-translation stage and the other is connected to a force sensor of FUTEK LPM200 panel mount load cell. The force controller performs to control the tensile force of micro-scale fibrous materials pulled by one clamp and to measure pulling force by the force sensor installed on the other clamp. By doing so, it can obtain more exact data of mechanical property of the micro-scale fibrous materials depending on the input target force.

For the implementation of the force feedback controller, the conventional Proportional-Integral Derivative (PID) and Proportional-Integral (PI) controls are used for the tensile test simulation due to its simple structure and design, low cost and high performance. A computer model of the microrobotic platform is built based on its mathematical models. In order to find usable controller parameters, conventional rule based tuning methods such as Ziegler Nichols, Pessen Integral of Absolute Error (PIAE), Some overshoot rule (SO-OV) and No overshoot rule (NO-OV), and Simulink PID tuner are utilized for the computer model. Finally, the force feedback controller is applied to the real microrobotic platform to compare the differences of the behaviors of the open loop system and the force feedback control system as the closed loop.

PREFACE

This thesis work has collaborated with the Micro- and Nanosystems Research Group at Department of Automation Science and Engineering, Tampere University of Technology since Jan of 2016. First of all, please let me give my special thanks to Prof. Pasi Kallio because he gave me opportunity for the thesis work and has sincerely supported me during this work. Also, I want to express my gratitude to Mathias von Essen and Markus Kakkonen who have helped to proceed my thesis work with their knowledge which made me to sustain the required perspective to proceed the thesis work.

I would like to thank to my family, especially my parents Donghyun Kim and Okyeon Jang who has supported throughout my life. My sisters, Enja Kim who led me to continue my studies in Finland and Minyoung Kim who has been always good friend to me. I am also grateful to my lovely daughter, Yeon Kim who are always bright and healthy. Finally, my dear, Jungmi Cha. Without her sincerely help, I would have not finished my master 's degree. I strongly believe that I was born to love you and let’s walk our life together like now.

Espoo, 14.12.2017

Taehoon Kim

CONTENTS

LIST OF FIGURES

LIST OF SYMBOLS AND ABBREVIATIONS

AFM	Atomic Force Microscopy
Back EMF	Back Electro Motive Force
CW	Clockwise
CCD cell chip	Charge-coupled device cell chip
CCW	Counterclockwise
D	Derivative
DC motor	Direct current motor
DOF	Degree of freedom
DG	DC gear motor
FHTB	Free-falling Hopkinson tensile bar
FIR	Finite impulse response
FOLPD	First order lag plus delay model
FOV	Field of View
I	Integral
IPF	Individual papermaking fibers
ISDG	Interferometer strain/displacement measurement system
LD pump module	Laser diode pump module
LED	Light emitting diode
Max	Maximum
MEMS	Microelectromechanical systems
MEM	Microelectromechanical
MG	Microgripper
Min	Minimum
MP	Micropositioner
NO-OV	No overshoot rule
PD	Proportional Derivative
PI	Proportional Integral
PID	Proportional Integral Derivative
PIAE	Pessen Integral of Absolute Error
PVDF force sensor	Polyvinylidene fluoride force sensor
PWM	Pulse-width modulation
RG	Research Question
SEM	Scanning Electron Microscopy
SO-OV	Some overshoot rule
VCM	Voice coils motors
ZPETC	Zero-phase error tracking controller

A	*Cross sectional area of fiber*
B	*Proportional factor*
c_b	*Wave speed in the bar*
D_l	*Delay time*
D_{ead}	*Deadband*
d	*Total displacement by motor movement*
d_t	*Displacement of the indenter*
d_f	*Elongation of the microfiber*
E	*Young's modulus*
e	*back EMF*

F	*Force to deflect the fiber*
F_d	*Desired force*
F_{in}	*Input force*
F_m	*Measured force by force sensor*
F_l	*Lateral force*
g	*Gravitational constant*
i	*Current*
l_0	*Half of the fiber length at the initial fiber position*
J	*Total inertia*
J_m	*Motor inertia*
J_l	*Leadscrew inertia*
J_{ls}	*Load inertia*
K_d	*Coefficient for the derivative term*
K_e	*Back EMF constant*
K_i	*Coefficient for the integral term*
K_p	*Coefficient for the proportional term*
K_u	*Ultimate gain*
K_t	*Motor torque constant*
L	*Length of the glass fiber*
L_a	*Motor inductance*
L_{ls}	*length of leadscrew*
p	*Pitch of DC motor shaft*
r	*Radius of the glass fiber*
R_a	*Motor resistance*
R_{ls}	*Radius of leadscrew*
T_m	*Motor torque*
T_a	*Acceleration torque*
T_f	*Friction torque*
T_d	*Derivative time*
T_i	*Integral time*
T_l	*Load torque*
u	*Particle displacement along fiber axial direction*
V	*Voltage*
V_d	*Driving voltage*
w_m	*Angular velocity of DC motor shaft*
W_{ls}	*Weight of leadscrew*
W	*Carriage with load*
w_{out}	*Output of backlash block*
x	*Travel distance of the cantilever*
Δy	*Distance of fiber deflection*
σ	*Fiber tensile stress*
ε	*Fiber tensile strain*
ε_i	*Incident strain*
ε_r	*Reflected strain*
ρ_{ls}	*Density of leadscrew*
P_d	*Desired position*
P_m	*Measured position*
P_e	*Position error*
T	*Time constant*

T_d	*Desired torque*
T_s	*Measured torque*
T_e	*Torque error*
θ	*Angle*
Δl	*Change in length of fiber*

1 INTRODUCTION

This master's thesis examines the technological solutions to implement the force feedback control in the microrobotic platform for the tensile testing of the micro-scale fibrous materials. This chapter provides the motivation of the thesis with the objectives and contributions. Afterward, the structure of the thesis is defined.

1.1 Motivation

The force control has been a well-known solution in a robot industry requiring more and more robust and accurate object manipulation for past three decades [1][2][3][4][5]. In the micro- and nano scale material testing application, it has been actively utilized especially for the two-fingered micromanipulation system to control the gripping force while the system grips deformable biomaterials or micro- and nano scale objects for manipulation and characterization [5][16][10-17]. However, the author argues that it has not been used for the tensile testing application of the micro- and nano scale fibrous materials despite its importance.

For the tensile testing of micro- and nano scale specimens, the tensile testers and machines have been typically used and developed. They can be categorized into three types such as load cell based micro-tensile testing machines [20, 25-34], Atomic Force Microscopy (AFM) with the nano-indenter [18] and the special cantilever [32][33], and micro-tensile testers made for target applications [23, 37-41]. As one step forward, micro- and nano system technology group in Tampere University of Technology developed the microrobotic platform to measure the mechanical properties of the micro-scale fibrous materials such as in an individual paper fiber [23][24] and fiber bond [21]. It was meaningful study in fact that it represented new application of the microrobotic technology unlike its general application areas such as optical fiber [8][9][11][12], micro part [10], living cell [14][15][41], micro-size thin film [37][38], carbon nanotube and nanowire [39]. Furthermore, it could be able to resolve the problems occurring during the manual tensile test, such as wasting time to prepare the specimen for the test, and structural change of the specimen due to the human error [21][23][24].

This thesis work introduces new application of the force feedback control in the existing microrobotic platform designed for the tensile testing of micro-scale fibrous materials. By doing so, it expects to obtain more exact and reliable measurement of mechanical properties of the fibers and can also contribute to improving the quality of the final product in different fiber-based industries in the end.

1.2 Objective and Contribution

The main idea of this thesis work is to implement the force feedback controller in the existing microrobotic platform to control the tensile force according to the target force as the input and measured force as the output. The following research questions (RQ) are addressed in this thesis work.

RQ1. Which force control approach can be applied to the micro-tensile testing of the micro-scale fibrous materials?

RQ2. Is there any micro-tensile testing machine or testers usable for target application of this thesis work?

RQ3. How can the force feedback control be applied to the microrobotic platform designed for the micro-tensile testing of the micro-scale fibrous materials?

The contributions of the thesis are described as below.

- The computer model of the microrobotic platform with the force feedback control is designed and implemented for the tensile testing simulation.
- The current behavior and limitation of the microrobotic platform during the micro-tensile testing are analysed.
- The force feedback control is implemented in the microrobotic platform for the micro-tensile testing of the micro-scale fibrous materials.

1.3 Outline of the Thesis

The thesis has following structures: Chapter 2 offers the theoretical background on general methods and applications of the force control, and testing methods and platforms for typical micro-tensile testing. Chapter 3 provides the user with details of research methods and materials used in this thesis work such as technical requirements and the implementation of the microrobotic platform and its computer model with different tuning methods. Experimental result and discussion are described in Chapter 4. Chapter 5 is for conclusion of the thesis work.

2 THEORETICAL BACKGROUND

This chapter offers the theoretical background in the force control including general methods of the micro-scale tensile test and testing platforms for different applications. Specifically, Section 2.1 provides the understanding of force control and describes currently used methods and applications. This section is a reference for building the force feedback controller in the microrobotic platform. Section 2.2 deals with typical tensile testing methods in micro- and nano scale specimens. It also introduces various methods and testing platforms in the different applications.

2.1 Force Control

The force control has been playing a fundamental role to achieve the accurate and robust manipulation in unforeseen situations such as the disturbance as it offers the intelligent response with the enhanced interaction between the robot manipulator and the environment [1][2][3][4][5]. The pure motion control is not able to guarantee such sophisticated manipulation due to the limitation to perform desired and planed manipulation tasks. In case of the physical contact task, it can be characterized by the dynamic interaction between the robot and environment such as inertia or elasticity. The pure motion control cannot manage such task because any modeling errors and uncertainties are able to trigger the unreliable behavior during the interaction without the force feedback loop and force control [1]. The feasible way to reach the requirement excluding the force control is to build accurate models of the robot manipulation, by kinematics and dynamics, and environment such as geometry and mechanical features. However, obtaining exact parameters to build such model is still challenge in a way that in practice, planning errors for the manipulation task gives rise to the deviation between real trajectory and desired one [1][5]. Furthermore, in the manipulation task in micro- and nano scale, it is one of the main challenges to achieve the efficient and safe gripping tasks without the damage to the specimen. For this reason, it requires the force feedback loop and force control to interact between the actuation and the measured force in such tasks. Many studies have been suggesting to employ the force control as the realistic solution [1][2][4][5][16].

Section 2.1.1 describes the general methods of the force control typically used in the robot industry. Section 2.1.2 offers major disturbances occurring during the force controlled manipulation task in micro-scale. The application areas of the force control are also introduced in Section 2.1.3.

2.1.1 Force Control Methods

Based on the history, the position control has been utilized in the simple robot manipulation task such as the spray painting and the welding, etc. because the interaction between the manipulator and the environment was not major requirement in such tasks. However, it has been shown that the need for the manipulation task requiring high interaction has been increasing, which pure position control cannot meet. In this regard, the force control has been well-known solution in such application as its interaction control

offers sufficient accuracy. In following sections, fundamental methods of the force control used in robot industry are introduced and are categorized into two different types such as passive and active force controls [1][2].

Passive Force Control

The passive force control relies on the inherited compliance mechanism of the robot and changes the trajectory of the end-effector by the interaction force due to the compliance [1][2]. In other word, the programmed trajectory is not changed unless its operation is finished. This passive approach is suitable for those requiring cheap and simple control systems with the fast response because it does not need force or torque sensors.
It also performs faster than that of the active force control approach as it depends on the compliance mechanism while the active approach does the reposition by the algorithm of the computer control [1]. However, some drawbacks of the passive force control are visible. It has the lack of the flexibility to perform different manipulation tasks due to the difficulty to design the passive compliance for each task. It also has small range of the position, orientation deviation and possible high contact force due to missing force measurement [1]. Therefore, it is difficult to use the passive force control in this thesis work because one of main targets is to compensate the disturbance detected by the force sensor on the fly.

Active Force Control

The active force control adjusts the trajectory of the end-effector by measuring the force. In other word, the force feedback control is considered to be mandatory to build proper control strategy in the approach. The active force control has strong advantages regardless of the real control implementation. Parameters of the force controller are easily adjustable whenever it needs to modify the parameters during the manipulation work. This benefit also leads to overcome the drawbacks of the passive force control. For this reason, the major robot manufacturers producing the industrial robot have already considered the capabilities of the active force control as the alternative solution [1][2]. However, it also has some disadvantages such as slower, higher cost and more sophisticated than those of the passive force control [1]. Especially, some level of the combination with the passive compliance is necessary to maintain the reaction force under the acceptable level. The reason is that the force feedback control is operated only if some motion and force error happens. Then, it can obtain reasonable running time for the manipulation task and reach the disturbance rejection [1]. Regarding to the implementation of the active force control there are two different approaches to proceed. First approach is called to the indirect force control and the other one is the direct force control [1][2].

Direct and Indirect Force Control

Typically, it requires three behaviors to perform the manipulation task for each direction of the operation space [3]:

1) Contact with the environment
2) Unconstrained movement to desired position
3) Intermediate or transitional behavior

For the robot manipulator, following two approaches can be used to implement the active force control [1][2][3][4].

A first approach is the indirect force control which can be implemented by using position or motion controls [1]. Figure 1 shows the block diagram of the position-based force control as the indirect force control. Please refer to Figure 1 as below.

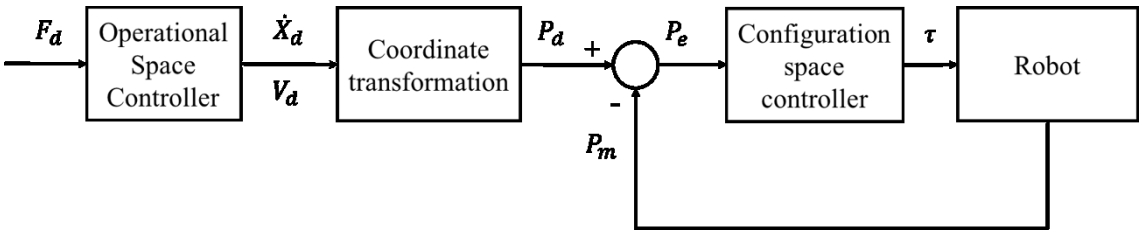

Figure 1. *Block diagram of Indirect force control*

In Figure 1, where F_d is the desired force. $\dot{X}_d$ is desired velocity of continuous time domain and V_d is desired velocity of discrete time domain in the operational space. P_d, P_m and P_e are the desired position, the measured position, and the position error in the configuration space, respectively. The configuration space controller produces τ to control the robot motors by the desired voltage and current [3]. The operational space can be defined by the Cartesian position and orientation of the robot end-effector by Euler angles. The configuration space means the space of all configurations specifying the all positions of the robot system.

The operational space controller generates the desired velocity $\dot{X}_d$ in order to perform the indirect force control. Then, this velocity is converted to the desired position P_d via the coordinate transformation block. The desired position P_d is eventually achieved by the motor of the robot controlled by the configuration space controller [3]. In the position-based force control, it requires the position controller from the robot manufacturers as only force and torque sensors are major parts to be modified in the hardware level. Those sensors are the mechanical standard to guarantee the reliability while the manipulator interacts with environment. In other word, it can change the reference position of the position controller to achieve the desired interaction between the force and the mechanical impedance. Therefore, the position-based force control has been significantly used because the architecture of the controller is not affected by other external modifications [2].

The direct force controller consisting of two loops. The external loop is the force control, and the internal one is the torque control [3]. Figure 2 represents the block diagram of the direct force control, where T_d, T_s and T_e are the desired torque, the measured torque, and the torque error in the configuration space, respectively.

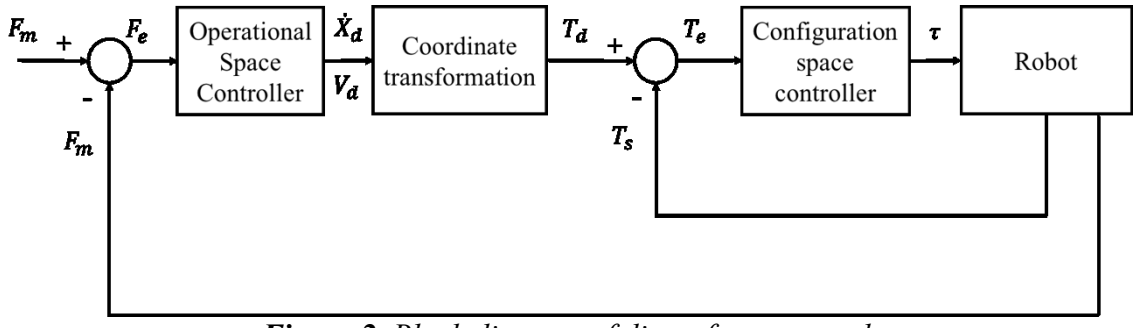

Figure 2. *Block diagram of direct force control*

The aim of the internal loop is to achieve the desired torque for each joint generated by external controller dealing with the manipulator dynamics. It executes under the condition that dynamics is known. It calls the torque-based force controller [2][3]. One drawback of the torque-based force controller is that it is much more difficult to implement than that of the position-based force control as it requires major modification in the controller. Basically, to achieve desired robustness against model uncertainty and deviation, it is compulsory to build the suitable controller design under the exact model of the manipulator dynamics [2][5].

Impedance Control

The impedance control was presented by N. Hogan in 1984 due to the nature of the manipulation requiring the mechanical interaction between the manipulator and the environment [6]. In principle, the impedance control means to regulate the relation between the force, and the position, the velocity and the acceleration. In this sense, it controls the impedance of the mechanism and generates the force output according to the motion input such as the position, the velocity and the acceleration. The reverse of the impedance is an admittance. the admittance control accepts the force input and yields the motion output such as the position, the velocity and the acceleration [5][6]. Please refer to Figure 3 as below.

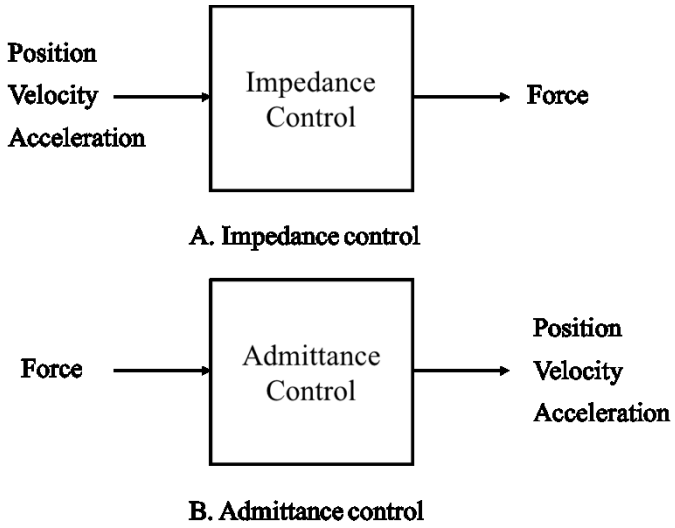

Figure 3. *Simplified block diagrams of the impedance and admittance controls*

In most cases of the manipulator task, the admittance can be considered as the environment because it includes inertia's and the kinematic constraints, i.e. it consists of two physical systems to accept the force command to detect the position, the velocity or the acceleration. Based on this, the manipulator is considered as the impendence because it accepts the motion command to find necessary force and torque [5][6]. Main aim of the impendence control is the stable interaction between the manipulator and the environment and it can be achieved by defining dynamic relation between the applied force related to the impedance and the position of the end-effector [5][6]. Since the impedance controller relies on the reference of the position commands, it can be used with the position feedback loop as well as the force feedback loop [5][6].

2.1.2 Force Control Applications in Micro-scale

In the applications of the force control in the micro- and nano scale, the two-fingered micromanipulation systems have been significantly utilized with the integrated force sensor to measure and control gripping force to manipulate and characterize the deformable biomaterials and the micro- and nano scale structures. The two-figured micromanipulation consists of two mobile manipulators and the control system to perform more sensible task by cooperative control [5][10-17]. Although research about contactless manipulation in the micro- and nano scale due to an advantage of non-adhesion force between the object and the manipulator has been performed, the mechanical contact to manipulate the object is still more common approach than the contactless one because the contactless manipulation could not be used for the gripping force control due to the lack of blocking force applied to the object [7].

In general, the two-fingered micromanipulation system consists of the following structures to measure and control the gripping force [16]:

1. Actuation mechanism: this mechanism consists of the actuated fingers and the object is grasped by them.
2. Measuring mechanism: this mechanism measures position and/or gripping force executed by the fingers.
3. Controller: it is for controlling the gripping force by the fingers.

The chronological overview of the two-fingered micromanipulation system aforementioned is described as follows.

A first micro manipulation system using the PI controller for the gripping force feedback mechanism was introduced by M. C. Carrozza et al in 2000 [8] and A. Eisinberg in 2001 [9]. It included microgripper (MG) built with the piezoelectric actuator and strain gauge glued on the MG. The PI controller was used to control the gripping force and the position of actuated MG to manipulate the contacted object as shown in Figure 4 [8][9].

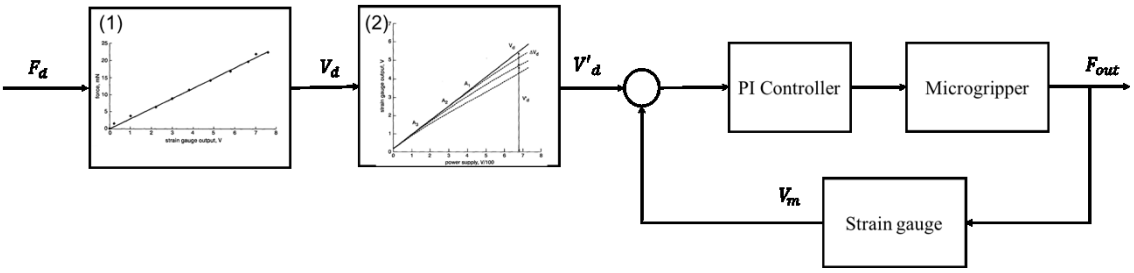

Figure 4. *Block diagram of force feedback control system, (1) Gripping force against output signal of strain gauge, (2) Output signal of strain gauge in idle and grasping conditions [9]*

Following procedures were performed for the force control [9].

1) Impose the desired force (F_d).
2) Calculate the corresponding strain gauge voltage (V_d).
3) Determine the output signal (ΔV_d) of the actual strain gauge while the MG grasps the object.

4) Use the signal V'_d $(= V_d - \Delta V_d)$ as the input for the PI controller.

To control the gripping force, an optical fiber was used as the object and it was supplied by the gripping force of 1.2 mN amplitude and ≈ 122 μN measurement noise [10, 11].

In 2000, Y. Zhou and B. J. Nelson showed the P controller to control the gripping force by the MG including two AFM cantilevers in Figure 5 [10].

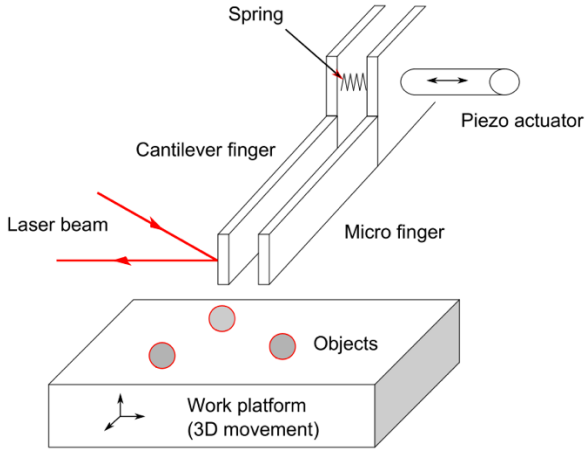

Figure 5. *Microgripper using two AFM cantilevers [10]*

The first cantilever can be moved by the piezoelectric actuator. The other one performed as the force sensor. the deflection was measured by using a photodiode. The calculation of the applied force was done by multiplying the measured deflection [10]. Then, the P force control law was used to control the desired contact force. The manipulated object size was less than 100 μm and, 100 to 200 nN gripping force was used to handle the micro-objects. This system measured 2 nN force (min) [10].

In 2004, D. H. Kim et al proposed the force feedback control for the manipulation system using the polyvinylidene fluoride (PVDF) force sensor. The force sensor was embedded in the MG for the assembly of the optical micro-component [11]. The strain gauges attached to the first actuated gripper was utilized for the position measurement. The other strain gauge mounted on second sensing gripper was employed to measure the gripping force. Then, the force feedback controller controlled the gripping force to fit a lensed optical fiber into laser diode (LD) pump module [11]. The size of the manipulated optical fiber was 230 μm in diameter. The measured gripping force was 3.2 mN (min) and the noise was 300 μN [11].

In 2005, J. Park et al applied an adaptive zero-phase error tracking controller (ZPETC) to control the force of the MG on which the strain gauge was fixed as illustrated in Figure 6 [12]. This manipulation system dealt with 230 μm in diameter of the optical fiber and measured 3 mN (min) gripping force. This article claimed that following issues could be triggered if the feedback loop was only utilized. Firstly, it required to properly tune the control parameters if there exists unstable gripping force by any disturbance in order to track the desired force profile [12]. Secondly, the tracking errors are able to damage the object during the gripping work due to the excessive force which is bigger

than the reference force. It argued that above issues could be resolved by the adaptive ZPETC [12].

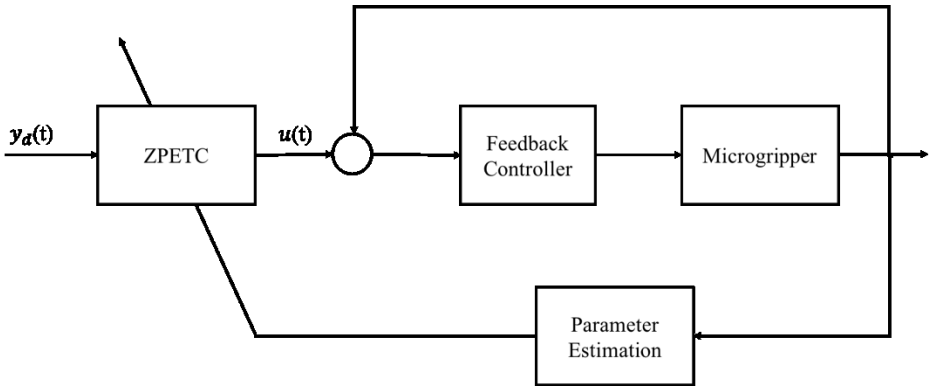

Figure 6. *Simplified block diagram of force control system with adaptive ZPETC [12]*

The ZPETC is the pole/zero cancellation and the phase cancellation based feedforward controller or the precompensator originally proposed by M. Tomiruka in 1987 [13]. Due to feedforward nature, it said it guaranteed better tracking performance than those of other controllers [13].

In 2008, K. Kim et al showed the PID feedback controller in the manipulation system including a monolithic Microelectromechanical (MEM) based MG. It was actuated by void coil motor (VCM) actuator with embedded two capacitive force sensors [14]. Please see Figure 7 as follows.

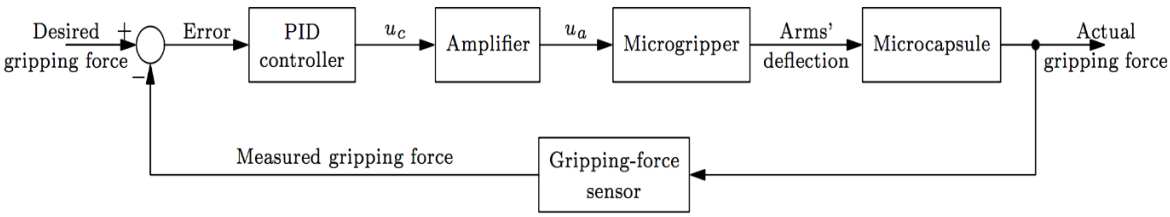

Figure 7. *Block diagram of the PID force feedback controller [14]*

A first force sensor had 38.5 nN as theoretical force resolution and was used for the contact detection. The other allowed the measurement of the gripping force with 19.9 nN theoretical force resolution. It demonstrated micro-Newton force level in the gripping force control. The biomaterials of around 20 μm in diameter was used for the manipulation and 2 μN gripping force (min) was applied to the biomaterials [14].

The first nano-Newton gripping force control with the improvement of the signal to noise ratio of the measurement was achieved by X. Liu, et al in 2009 [15]. In this platform, microelectromechanical systems (MEMS) based MG was used to manipulate the object and to provide desired gripping force signal by the mechanism of the integrated PID force feedback control. Interstitial cells of around10-20 μm in diameter were utilized for the manipulation and the controlled gripping force was 60 nN (min) [15].

2.1.3 Disturbance Rejection in Micromanipulation

The micro-scale force control in the manipulation task is more complicated than that of macro system [16][17]. Normally it is a challenge to master a micro manipulation task in terms of the gripping force control and the measurement because of the following reasons [16].

1) Complexity of nonlinearity of actuation dynamics in the micro-scale.
2) Low ratio between the data signal and the noise.
3) Adhesion and attraction phenomena in the micro-scale.

Especially, the noise is the major disturbance to be concerned during the grasping task because it causes the degradation of the performance and stability of the force control, and uncontrolled force to the object. Articles [16] and [17] suggested the disturbance rejection based force control approaches to resolve the issue aforementioned.

In 2014, M. Boudaoud and S. Regnier showed the grasping force control with the concern of the noise disturbance rejection. It argued that increasing noise level was the issue in grasping because it causes that MG is not possible to detect the object [16]. This effect triggered to decrease the resolution of the gripping force, i.e. it became the state where there was no any change on signal amplitude measured by force sensor no matter whether it was before or after grasping due to the noise amplitude [16]. Therefore, this article suggested the way to reject the noise. First of all, it required to implement proper noise model to deal with it and to come up with the strategy for noise rejection. Secondly, the article said that it required the robust controller to guarantee the stability of uncertainties against the mechanical properties of the manipulated object [16].

In 2015, H. Ghafarirad et al introduced the disturbance rejection of the force control approach by the piezoelectric actuators. It used the disturbance observer to estimate the disturbance [17]. This approach is shown in Figure 8 as below.

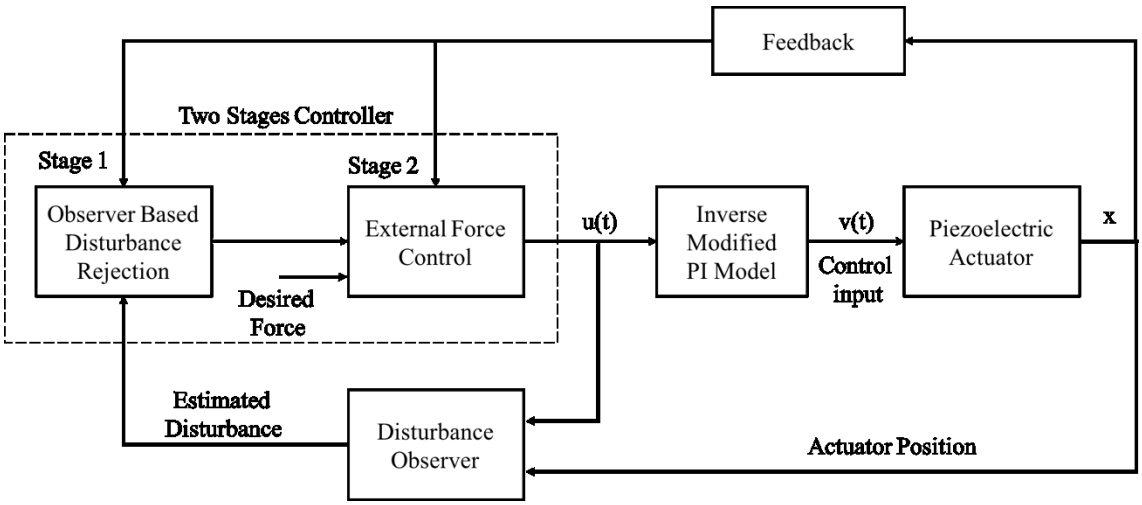

Figure 8. *Block diagram of force control approach with disturbance rejection [17]*

The disturbance observer did not limit estimated disturbance bound, i.e. regardless of the disturbance magnitude, the disturbance was measured and balanced by the disturbance observer. Thus, the disturbance observer was employed for measuring the existing

disturbance and the feedforward compensation. The free disturbance of desired dynamic model was achieved by robust sliding mode controller removing the estimated disturbance [17]. This approach included two stages. Stage 1 was an observer-based robust control for the disturbance rejection. Specifically, it introduced the disturbance observer to estimate disturbance with no relation to its magnitude and then estimated disturbance was utilized for the feedforward disturbance system. Stage 2 was the external force control against the unknown environment [17].

2.1.4 Summary

Table 1 offers the main characteristics of the two-fingered micromanipulation systems to control the gripping force, mentioned in Section 2.1.2. It shows different combinations of the force controllers and sensors to manage the various range of the gripping force from a few nano-Newton to hundreds micro-Newton. Based on Table 1, the P, PI and PID controller were still mainly used to control the gripping force due to its simplicity, clear functionality and applicability. Each controller of the system is used to obtain the mechanical property of the individual specimen. However, it should be careful when applying the certain controller for another specimen because it is already specified for certain specimen and another specimen may have different mechanical properties such as its size and stiffness, e.g. biomedical sample [16][15].

***Table 1**. Summary of characteristics of the two-figured micromanipulation systems*

Force sensor type	**Gripper/Actuator type**	**Controller type**	**Application area**	**Measurement performance/noise**	**Gripping force max/min**	**Year**	**Ref.**
Strain gauge	Piezo electric	PI	Optical fiber	*/$\approx 122\mu N$	$22mN$/1.2 mN	2000/ 2001	[8] [9]
Photodiode	piezo electric	P	Micro object	> $1nN$(resolution)/$0.03nN$	$200nN$/$2nN$	2000	[10]
PVDF	VCM	Force feedback	Optical fiber	$39.6mN$/V(resolution)/$\approx 150\mu N$	$60mN$/$3mN$	2003	[11]
Strain gauge	VCM	ZPETC	Optical fiber	$12.82mN$/V(sensitivity)/*	$23mN$/$3mN$	2005	[12]
Capacitive	V-beam electro thermal	PID	Biomaterial	$19.9nN$(resolution)/$500nN$	$50\mu N$/*	2008	[14]
Capacitive	V-beam electro thermal	PID	Biological cell	$19.9nN$(resolution)/*	$50\mu N$/$60nN$	2010	[15]

The notation "*" represents that the characteristic is not offered in the reference.

From Table 1, it is noticeable that optical and electrostatic sensors support high resolution to measure nano-Newton level of the gripping force. In this sense, it leads to control nano-Newton level of the gripping force. On the contrary, the gripping force measurement of the strain gauge and PVDF measurements are 1.2 mN (min) and 3 mN (min), respectively. Thus, there is the resolution gap between them with the optical and electrostatic sensors. It needs to be aware that to control the nano-Newton level of the gripping force, it requires the force sensor performing the nano-Newton resolution and the micromanipulation system should be also able to perform the nanometer level of displacement [16][10].

In the micro-scale force control, the noise is the main disturbance interrupting the gripping force control and measurement. The noise level is normally bigger than theoretical resolution, i.e. the noise magnitude does not rely on working principal of the force sensor. Thus, the noise magnitude varies depending on the applications or test environments, even though it uses same force sensor operating under same physical principle. None of the papers described the clear reasons triggering the noise. However, following reasons commonly affect the noise magnitude [16].

1) The influence of electric measurement chain.
2) The effect of the vibration of the MG on measurement resolution.
3) The influence of the environmental noise.

Regarding the influence of the environment noise, it can be confirmed by the studies such as [14] and [15]. Both papers used same force sensor. But [14] showed the force sensor could not measure below micro-Newton of the gripping force while [15] used the force sensor to control the nano-Newton level of the gripping force. Therefore, the suitable model of the noise rejection is required to manage the disturbance in control system [16][17].

2.1.5 Conclusion

The force control has been important role in the robot industry for stable and accurate manipulation work over the past 30 years. This is because it is able to compensate unexpected disturbance during the manipulation between the robot manipulator and the environment. On the micro-scale, studies about MG with milli-Newton level of gripping force already started in the early 90's for the manipulation of the rigid material. The two-fingered micro manipulation system appeared for micro- and nano Newton levels of the gripping force control and measurement afterward. The force control and general methods of the force control adapted to the industry are explained. In addition, the overview of two fingered micro manipulation systems performing the gripping force control by the micro- and nano scale materials is also described. In the future, the interest to manipulate by nano-Newton force control will increase. To achieve this, the manipulation system should have the force sensor performing nano-Newton force resolution and the competence to control nano-Newton force with the proper noise rejection strategy.

2.2 Micro-scale Fiber Tensile Testing

The micro-scale fibrous materials have been considerably investigated in various application areas such as industrial sectors and biomedical applications. The reason is that close understanding on the mechanical characteristic of the fibrous materials is one of important factors for the product development and its quality [18-23].

In case of web or matrix based bulk materials, many equipment or tools have been developed to investigate their mechanical properties and they are commercially available. However, the mechanical properties of the bulk material are not sufficient to explain the mechanical property of the individual micro-scale fibrous material. In other word, it requires additional work to interpret this data from the bulk materials to grasp individual

one. Another important factor is that the tensile testing equipment and tools should ensure repeatability and high performance of the testing to obtain reliable data. However, the existing equipment and tools are still missing such requirements. It requires the user to spend the significant time and effort in preparing fiber specimen manually for the tensile testing [21][23]. Therefore, customized tensile testing equipment and tools designed for certain use case have been implemented to overcome the drawback [23][37-41].

Following Section 2.2.1 and Section 2.2.2 presents information on individual micro-scales fiber materials and the specimen preparation, respectively. Section 2.2.3 offers the common methods of the micro-tensile test used for past three decades.

2.2.1 Micro-Scale Fibers

Since the dimensions of micro-scale fibrous materials deviate from a few micrometers to hundred micrometers, it is more difficult to manipulate and characterize the individual micro-size fiber than that of the bulk materials such as web or matrix types [18-23]. However, once the tensile testing with the individual micro-scale fiber is successfully performed, it is possible to estimate its mechanical property, which is the essential factor to understand the structural integrity of the specimen. Eventually it leads to improve reinforced structure of the final product [18-23]. For example, the biodegradable polymer as the micro-scale fiber is often utilized for tissue regeneration of the tendon, the ligament and the nerve. As in situ deformation of the tissue occurs in small strain level, it is considerably valuable to grasp the mechanical property of the single fiber under the small deformation [18]. In case of papermaking fiber, obtaining new information and data about fiber and fiber wall fine structure provides an opportunity to improve the quality of the paper and the pulp in the end [23].

2.2.2 Specimen Preparation

The specimen preparation is known as the laborious work requiring significant time consumption and skilled and experienced personnel. The techniques of the sample preparation are categorized to the types of mounting, either temporarily or permanently, and the types of biological and non-biological specimens. In the fields such as the unwoven material, the pulp and the paper, the composite materials and the optics, understanding the mechanical behaviors of the fibers are important to make the product with the high quality [23][24].

During the preparation of the micro-scale fibrous materials, the key is to ensure that there are no any artifact and structural changes in the specimen, which normally occur by human error during the handling [23][24]. Furthermore, it is more difficult to deal with the micro-scale material than that of macro-scale due to the much higher aspect ratio of the material. Normally its diameter is around tenths of micrometers and length is about a few millimeters [23][24]. These problems can be resolved by the microrobotic platforms as it performs the manipulation task including the specimen handling itself with high throughput. Therefore, the microrobotic technology has been significantly used in diverse applications to manipulate micro- and nano scale specimens such as optical fibers [8][9][11][12], micro parts [10], living cells [14][15][41], micrometer-sized thin films [37][38], carbon nanotubes and nanowires [39]. Some studies showed that the

microrobotic platform was used for characterizing the flexibility of the micro-scale individual paper fiber [23][24] and the fiber bond [21].

2.2.3 Micro Tensile Test Method

The tensile testing tester is designed testing platform for investigating the mechanical properties of the micro-scale specimen. The properties such as the tensile strength, breaking strength and maximum elongation are measured via the micro-tensile testing. In micro- and nano scales, the micro-tensile testers should support the measurement of the mechanical property of the specimen with the high repeatability. The measured data should be applicable to the product design and the performance estimation [23][24]. However, the smaller the size of the specimen has been, the easier breaking the specimen is during the handling. It means that it becomes more difficult to uniformly load the force to the specimen [23][24]. Moreover, since the accuracy of the mechanical behavior relies upon the accuracy of the specimen measurement, it requires the equipment supporting the high resolution. Therefore, the various measurement methods have been designed to meet the aforementioned requirements [23][24].

In general, there are three categories of the micro-tensile testers and machines to characterize the micro-scale specimens as follows [18]:

1) Micro-tensile testing machine using the load cell [20, 25-34].
2) AFM with the nano-indenter [18] and the special cantilever [32][33].
3) Micro-tensile testers created for target applications [23, 37-41].

Micro-Tensile Testing Machine Using Load Cell

The load cell based tensile testing machines are dealt with in this section. All tensile testing machines are used to obtain the mechanical property such as the tensile stiffness of the different specimens such as the thin film and fiber. First of all, the load cell based tensile testing machines using the thin film are introduced. Afterward, it deals with the tensile testing machines using the individual fiber.

- Tensile Stiffness Measurement for Thin Film

In 1989, W. Sharpe. Jr developed the interferometer strain/displacement measurement system (ISDG) obtaining mechanical property such as tensile stiffness of the thin film. It measures the force by the load cell and the strain by the laser sensor [29]. The ISDG was non-contacting option techniques to measure the strain or the displacement between two gauge markers reflected from the specimen surface [25][29][30][31]. Its optical principle basically followed the Young's two-slit interference, excluding a fact that it happened under the reflection rather than the transmission. When two gold markers deposited on the metal surface were reflected by the laser, the diffracted reflections by each gold were overlapped and interfered to produce the fringe. In other word, once the two markers moved during the deflection, the fringe pattern was also moved. This motion was measured by the photo sensor and was relevant to the change of the displacement by the strain [25][29][30][31]. Please see Figure 9 as below.

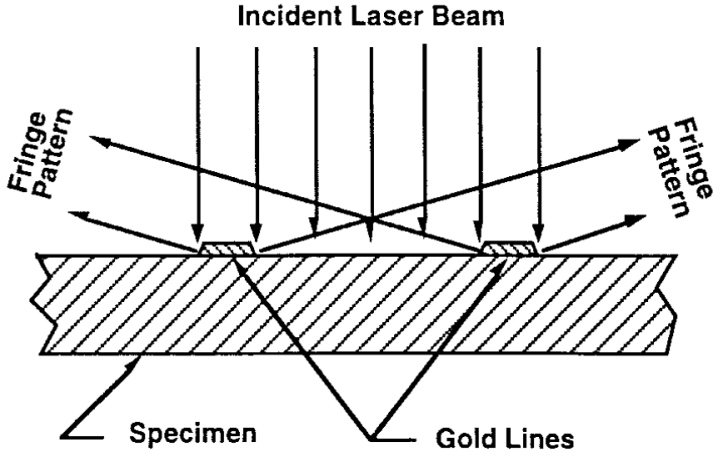

Figure 9. *Schematic of the ISDG [29]*

W. Sharpe. Jr introduced another method to get rid of the friction by using the air bearing for the accurate load measurement in 1997 [30] and improved the tensile tester to pull the specimen by mounting the load cell to single axis piezoelectric picomotor in 1998 [25]. In 2001, M. Zupah et al presented the micro-sample testing system including the high temperature. The testing system was capable gripping the section of the load frame and the load cell having the force range, 90 N and the resolution, 20 mN. By doing so, it could measure the mechanical property such as the tensile stiffness of the micro-sample under the various load levels within the wide range of the temperature [31].

In 2002, M. Haque and M. Saif introduced a MEMS-based uniaxial tensile testing technique by a MEMS load cell with the force resolution, 5 μN. It aimed to measure the in situ mechanical characteristics such as the tensile stiffness of nano-scale thin film [26][27]. The test setup consisted of the tensile test chip and the piezoelectric actuator. It was fabricated with the thin film fixed on the beam of the force sensor in the tensile test chip. Basically, the end of one side of the specimen was fixed to support the beam assembly while the opposite end of the side was pulled by piezoelectric actuator. Once deflection occurs, it was detected by the beam of the force sensor via the thin film [26][27].

A Study by E. Bamberg, et al introduced the load cell based tensile tester managing the resolution, 125 mN and the force range, 25 N in 2006. Depending on the controlled load condition, the stress-strain characteristics, i.e. the tensile stiffness of the polymeric micro- and nano size thin film could be measured [28]. To evaluate the microstructure and the mechanical behavior before and after the tensile testing, the AFM was used [28].

- Tensile Stiffness Measurement for Fiber

For the load cell based tensile testing using the individual fiber, the Hopkinson bar called Koskly bar has been utilized. In 2005, M. Cheng et al, tried to improve the original Hopkinson tensile bar to measure the mechanical property such as the tensile stiffness of the individual fiber [32]. The operational principle of the Hopkinson tensile bar was that the specimen was fixed on the middle between the incident bar and the transmission bar. Then, the collision was triggered on the end of the incident bar by the

striker tube. It generates the stress wave. Afterward, the stress wave propagated from the incident bar to the transmitter through the specimen. It measured the stress by the strain gauge installed in both the incident bar and the transmission bar. This article concluded that transmission bar in the conventional Hopkinson tensile bar was not sufficient to measure the low level of transmitted force, 0.5 N (max) due to the lack of the sensitivity. Therefore, M. Cheng replaced the transmission bar with the sensitive quartz transducer in [32]. Please refer to Figure 10 as below.

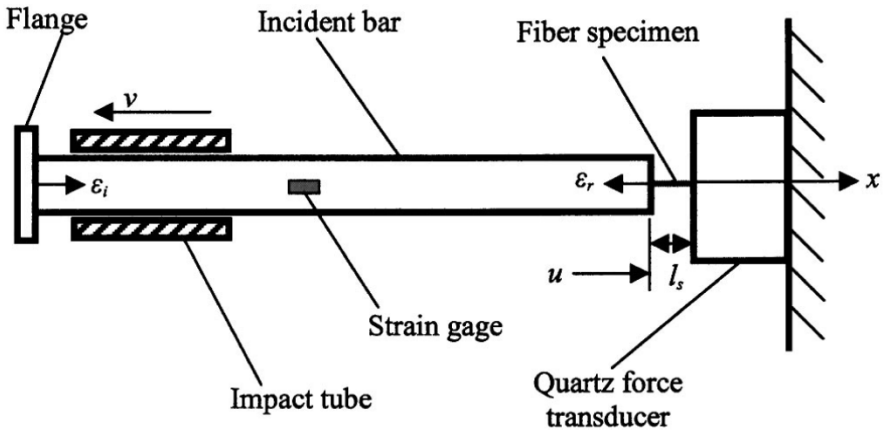

Figure 10. *Schematic description of Hopkinson tensile bar method for a single fiber measurement [32]*

Based on the theory of the one-dimensional wave propagation, the particle displacement u along the fiber axial direction, i.e. x direction in the incident bar was explained as below [32].

$$u = f(x - c_b t) + g(x - c_b t) \tag{7}$$

Where $f(x - c_b t)$ and $g(x - c_b t)$ were the function about the incident and the reflected wave shapes respectively. c_b means the wave speed in the bar [32].

The one-dimensional strain is defined by

$$\varepsilon = \frac{\delta u}{\delta x} \tag{8}$$

As the same value was shared by both fiber specimen and the incident bar at their interface, it used same notation for the x directional particle displacements. Thus, the particle velocity was described in Equation 9 [32].

$$\dot{u} = c_b(-f' + g') + c_b(-\varepsilon_i + \varepsilon_r) \tag{9}$$

Where ε_i is the incident and ε_r is the reflected strains. The strain rate of the fiber sample was defined as the particle velocity at the end of the incident bar by dividing length of the specimen l_s under the assumption that the fiber sample was under the condition of the dynamic force equilibrium [32].

$$\dot{\varepsilon} = -\frac{\dot{u}}{l_s} = \frac{c_b}{l_s}(\varepsilon_i - \varepsilon_r) \quad (10)$$

Then, the strain in the fiber sample as the function of time t could be represented by the integration in Equation 11 [32].

$$\varepsilon = \int_0^t \frac{c_b}{l_s}(\varepsilon_i - \varepsilon_r)d\tau \quad (11)$$

The study by J. Lim, et al in 2009 showed to use the quartz-piezoelectric load cell with the force range, 22.24 N rather than the transmission bar to measure the low-level force. In order to obtain the axial stress of the fiber, it required to divide the force by the fiber cross-sectional area [33]. In 2010, a miniaturized optical strain measurement system was presented by using the non-contact laser technique to measure less than 5% axial small strain during the fiber deformation [33]. In 2016, P. Wang proposed a miniaturized free-falling Hopkinson tensile bar (FHTB) to understand the mechanism of the failure occurring under the dynamic tensile loading of the individual carbon nanotube fiber [20].

Atomic Force Microscope (AFM) Based Tensile Tester

The AFM has been well used for measuring the mechanical properties such as the stiffness and adhesion of the specimen as it operates with both force and distance sensors. There are two common methods of the AFM to measure the mechanical properties. The first method is to perpendicularly move the cantilever to the plane of the specimen such as the nanoindentation. The second one is to bend the specimen such as the nano-size fiber. In all AFM force measurement, it utilizes the AFM cantilever to apply the force to the specimen during the investigation [35][36].

- Tensile Stiffness Measurement by Perpendicular Movement

As the first method, E. Tan and C. Lim developed an AFM based nano-indentation system to execute the tensile testing of the micro- and nano scale fiber with tens of milli-Newton force range with the resolution, 80 nN [18]. Due to the high resolution to measure the load and elongation of the specimen in this system, it allows to execute the small strain tensile testing of the microscale fiber (<0.1% gauge length). The standard material testing machines could not manage the tensile testing at the small strain due to poor resolution in the measurement [18].

The AFM-based nanoindentation system included a nano-indenter scanner, which continuously monitored the depth of the indent related to a surface of the specimen and the indentation load. Then, the mechanical properties such as Young's modulus and hardness could be gained based on a plot of the indentation load by the displacement on loading and unloading of the nano-indenter [18]. This study argued another way around of the system by changing the loading directions of the nano-indenter. For the tensile testing, the micro-size fiber was vertically glued on both the intender tip and the tip of a base plate as Figure 11. Then, the stepper motor of the AFM system stretches the micro-size fiber as the actuator [18].

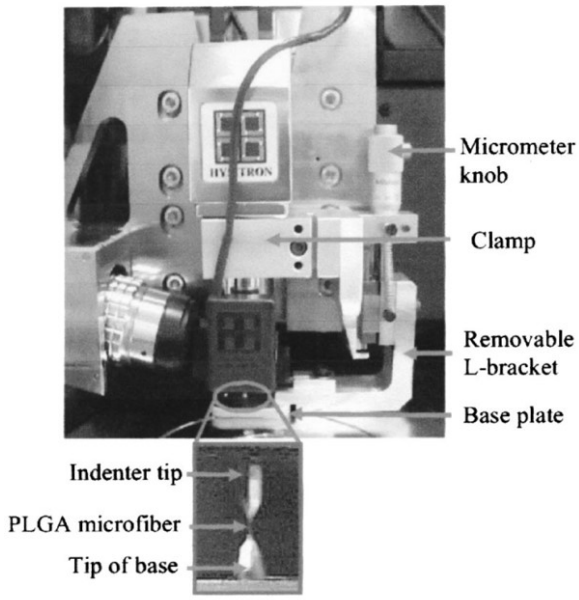

Figure 11. *Setup of nanoindenter on AFM-based nanoindention system [18]*

The elongation of the micro-size fiber was defined in Equation 12.

$$d_f = d - d_t \tag{12}$$

Where d, d_t and d_f are the total displacement by the movement of the stepper motor, the displacement of the indenter, and the elongation of the micro-size fiber, respectively. It was possible to calculate the strain of the micro-size fiber by dividing the elongation over the gauge length. Its stress could also be obtained by dividing the tensile load measured over the cross-sectional area of the micro-size fiber [18]. The article indicated limitations of this method such as the limited range to stretch the specimen. In practice, it had the limited load range around tens of milli-Newton (max), 5 μm limited elongation by the nanoidentation system and limited displacement rate by the speed of the stepper motor. It also showed the difficulty to prepare and to manipulate the micro- and nano scale fiber in the system and argued that the suitable micromanipulation is necessary in this system to resolve this [18].

- Bending Stiffness Measurement by Bending

As the second method, studies in [35] and [36] introduce the bending stiffness testing by the AFM to obtain the mechanical property of the glass fiber. W. Liu, et al proposed the tensile testing method using a AFM lateral force measurement in 2007 [35]. This tensile system fixed the end of one side of the glass fiber to the end of the one side of the substrate. Then, it laterally bended the other end using the AFM tip under the force range from 0.053 to 1.38 N/m. This method allowed to measure the applied force to the glass fiber and to understand its deflection characteristics. However, the AFM was mandatory to use this method, and the length of the tip must be determined in advance [35].

The common method of the AFM is to bend a fixed nano-size fiber by moving the cantilever vertically along the substrate plane. However, since the vertical motion range is limited in a few micrometers, it is difficult to arrive in the strength and elongation of breaking the fiber [36]. A. Gestos, et al in 2013 represented the horizontal motion based

method of the tensile testing for the individual electrospun nano-size fiber. It also proposed a method to fix the individual nano-scale fiber depending on a gap without additional fiber handling [36]. Please see Figure 12.

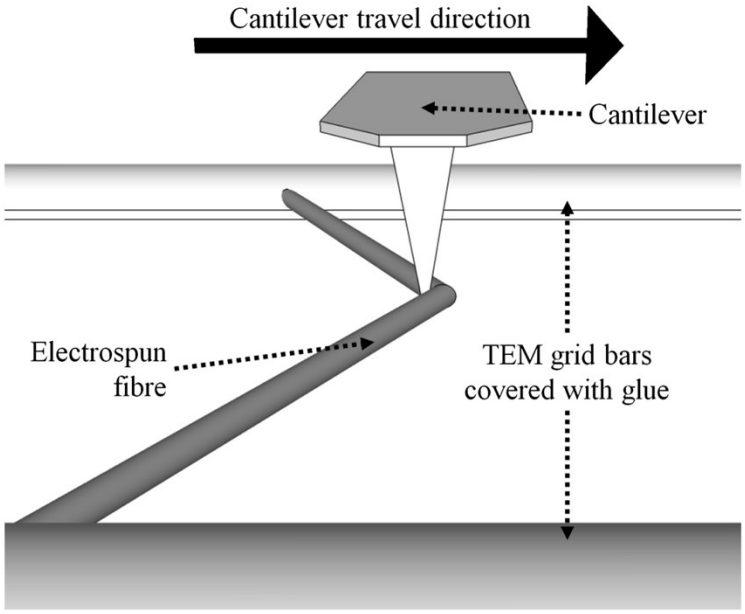

Figure 12. *Schematic diagram of the AFM cantilever for horizontal movement [36]*

To make the stress-strain curves, the following equations of the fiber tensile stress (σ) and strain (ε) is used to obtain the measured force against the cantilever travel curves during the experiment [36].

$$\sigma = \frac{F_l}{2Asin(\theta)} \tag{13}$$

$$\varepsilon = \frac{\left(\frac{x}{\sin(\theta)}\right) - l_0}{l_0} \tag{14}$$

$$\tan(\theta) = \frac{x}{l_0} \tag{15}$$

Where F_l means the lateral force measured in the cantilever, x denotes the travel distance of the cantilever from the initial fiber position to the stretched fiber one. θ and l_0 are the angle from initial fiber position to the stretched fiber one, and the half of the fiber length at the initial fiber position, respectively as illustrated in Figure 13 [36].

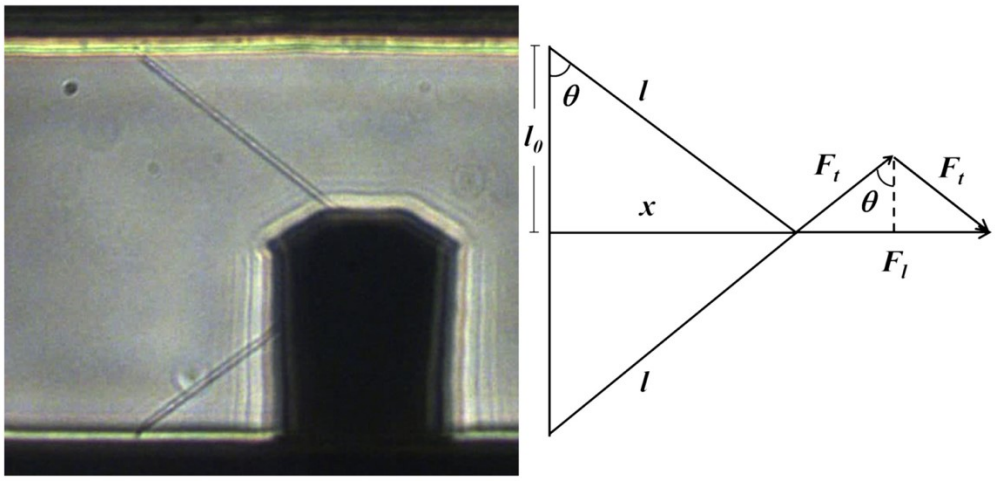

***Figure 13**. (Left) Optical microscope image of nanofiber stretched by the AFM cantilever, (Right) the simplified diagram indicating dimensions and resulting force, F_t is tensile force acting on each half of the fiber, $2l_0$ and $2l$ are the intial and final lengths of the fiber respectively [36]*

This lateral movement of the cantilever made it possible to perform the tensile testing for the suppressed fiber under the high strain rate and allows to grasp the mechanical properties of the individual nano-size fiber [36].

Micro-tensile testers created for target applications

The micro-tensile testers for target applications can be categorized according to the types of specimens such as the thin film, fiber and others such as the polymide substrate and muscle cell as below.

- Tensile Stiffness Measurement for Thin Film

T. Tsuchiya et al developed a different technique for high resolution in the micro-tensile testing rather than using the load cell in 2002. This system used the electrostatic force and the friction force to hold one side of the thin film and the other side fixed to a silicon substrate. It also supported a servo-controlled balance for the small force measurement. The system has the force range, 100 mN and the resolution, 1 μN [37].

In 2005, Y. Cheng et al produced the micro-tensile tester capable of measuring the tensile strength of the free standing thin film. This tester used an eddy-current displacement sensor with two steel stripes. The simple principle was to pull or push the brass bar and the string depending on the motion direction of the micromanipulator to generate the steel strip deflection. If this deflection changed the space between the eddy-current displacement sensor and the steel-strip assembly, a voltage occurs at this interval. Then, it was possible to observe the gap distance proportionally varying depending on this voltage. This system had 12 mN force range [38].

- Tensile Stiffness Measurement for Fiber

Y. Zhu and H. Espinosa developed a MEMS based tensile testing tester with 12 nN resolution and tens of milli-Newton force range in 2005. This system could characterize the properties of nano-size materials such as nanowires and measure the strength of the in-situ electron microscopy [39]. The system used the electrostatic comb drive actuators

for the sample loading and the thermal actuators for the displacement control. It also included the capacitance measurement based load sensors. Nanometer resolution of the system allowed to continuously observe the deformation and the failure of the specimen under sub nanometer resolution while it electronically measured the applied loads [39].

- Bending Stiffness Measurement for Fiber

In 2015, P. Sakati et al. presented the microrobotic platform to measure the bending stiffness, i.e. the flexibility of the individual papermaking fiber (IPF) and the chemical functionalization by the controlled manipulation. The principle of the microrobotic platform was to apply the force to the middle of the fiber beam grasped by two MGs. It utilized both-ends-fixed boundary condition of the beam theory for the flexibility measurement. As the microrobotic platform could guarantee high throughput and directly measure the flexibility of IPF, it could overcome the typical drawbacks of other tensile testers such as the time consumption for the specimen preparation and low yield. It also measured the flexibility of the IPF more accurately than that of the wet fiber by the confocal laser scanning microscopy or the flow cell based IPF [23].

- Tensile Stiffness Measurement for Other Specimens

Lastly, [40] and [41] reported a micro-tensile tester using a bender as a component of the force sensing to measure the tensile stiffness of the specimens such as the polymide substrate and muscle cell, respectively. In 2006, U. Lang et al used the silicon beam bender for studies of the polymer micromechanics. The force was detected by the deflection of the silicon beam and the strain of the specimen was measured by the optical detection such as a least square template matching algorithm (LSM) [40]. In 2007, K. Nagayama used a deflectable pipette for the analysis of the muscle cell viscoelasticity. It used pair micro tools such as the glass micropipettes and the microplates to deform the specimen [41].

2.2.4 Summary

Table 2 represents the summary of the different types of the tensile testers and machines for different applications with some characteristics for the tensile testing of micro- and nano scale specimens. They perform the force range from tens of micro-Newton to tens of Newton and the resolution from tens of nano-Newton to hundreds milli-Newton. In Table 2, It shows that the thin film had heavily been characterized for the tensile testing by the load cell based tensile testers. In Hopkins bar or AFM based tensile testers, it started to use micro- and nano scale individual fibers for the tensile testing.

Table 2. *Summary of the main characteristics of the Tensile Testers*

Tensile Tester	Actuator	Force/strain measurement	Force range/resolution	Application	Mechanical Property	Year	Ref
ISDG	Piezoelectric	Load cell/Laser sensor	$1N/200mN$	Thin film	Tensile stiffness	1989	[29]

	Piezoelectric	Load cell/Laser sensor	0.45N/5 mN	Thin film (35μm in thick)	Tensile stiffness	1997	[30]
	Piezoelectric	Load cell	90N/20mN	Micro sample (20-500μm in thick)	Tensile stiffness	2001	[31]
Load cell based	Piezoelectric	MEMS load cell	*/ 5μm	Nano-scale thin film (275μm × 100nm × 8.8μm)	Tensile stiffness	2002	[26] [27]
	Stepper motor	Load cell	25N/125 mN	Thin film (29.6mm × 5.0mm × 0.3mm)	Tensile stiffness	2006	[28]
Hopkinson Bar	*	Strain gauge	*/*	Individual fiber (12μm in diameter, 3.0/5.8 mm in length)	Tensile stiffness	2005	[32]
	*	Quartz-piezoelectric load cell	22.24N/*	Individual fiber (9.28±0.17μm)	Tensile stiffness	2009	[33]
	*	Strain gauge	0.1-0.001N/*	Carbon nano tube fiber (11.1±0.7μm)	Tensile stiffness	2016	[20]
AFM	Stepper motor	Nanoindenter scanner	Tens of mN/80 nN	Micro-scale Poly fiber (25μm in diameter)	Tensile stiffness	2004	[18]
	*	AFM	0.0053-1.38$\frac{N}{m}$/*	Glass fiber (100μm in length, 1μm in radius)	Bending stiffness	2007	[35]
	*	AFM	*/*	Nano-scale fiber (polymer)	Bending stiffness	2013	[36]

Electro-static force grip system	Piezoelec-tric	Weight measurement unit of ther-mogravimet-ric analyzer	100 mN/1 μN	Thin polysilicon film (500μm × 50μm × 2μm)	Tensile stiffness	2002	[37]
Micro-tensile tester	Motor	Eddy-current displacement sensor	12mN/∗	Thin film (180μm × 10μm × 1μm)	Tensile stiffness	2005	[38]
MEMS based	Electro-static comb drive	Load sensor	Tens of mN/12nN	Nanowire (20-30μm in length, 200nm in diame-ter)	Tensile stiffness	2005	[39]
Tensile tester by bender	*	By Silicon beam deflec-tion/Optical deflection	*	Polymide sub-strate (1μm in thick)	Tensile stiffness	2006	[40]
	piezo ce-ramic	Strain gauge	*	Muscle cell	Tensile stiffness	2007	[41]
Microro-botic	*	Capacitive Micro force sensor	10μN(ap-prox.)/*	IPF (0.8-4.5mm in length, 16-70μm in diameter	Bending stiffness	2015	[23]

The notation "*" represents that the characteristic is not offered in the reference.

In case of the micro-testing tensile machines using the load cell, they had been used as the standard test method together with the gripping device. However, a drawback is no-ticeable due to the difficulty to use for the thin film [21]. The Hopkins bar technique cannot be used for quasi static loading as its use case is to characterize the mechanical property at the high strain rate [20][32][33].

The AFM is popular tool to measure the mechanical properties of the micro- and nano scale specimen. However, it is not easy for the AFM to measure the strength and the elongation of breaking point of the specimen as the movement ranges of most AFMs are limited to a few micrometers. Also, the limitation of the force range and slowness dur-ing the micro-tensile testing are the other disadvantages of the AFM based tensile test-ing [18][36]. For these reasons, it has been shown that the micro-tensile testers for cer-tain application by microelectromechanical technology have been developed as the al-ternative solution [23] [37][38][39][40].

2.2.5 Conclusion

In the literature review, it deals with the overview of the general methods of the micro- and nano tensile testing which has been already utilized and developed for certain applications. Based on the survey of the studies aforementioned, it is able to comes up with the answers about the RQ1 and 2 in Section 1.2. The answer for the RQ3 is dealt with in Chapter 5.

RQ1. Which force control approach can be applied to the micro-tensile testing of the micro-scale fibrous materials?

From the literature review in Section 2.1, it is noticeable that in micro- and nano scale, the force feedback control has been well used in the two-figured micromanipulation systems to control the gripping force of the MG and to prevent the damage to the specimen during the gripping task as the active force control approach. As the aim of the thesis work is to implement the force feedback controller to control the tensile force during the micro-tensile testing, it is the different application area, compared with those of previous studies. However, those studies can still be valid as the references for the implementation of the force feedback controller in a way that it requires the force sensor to control the tensile force during the operation and therefore suggest the active force control approach as the method to implement. In addition, previous studies also suggested two technical requirements for the micro-Newton level of the force feedback control. First technical requirement is to accompany the force sensor performing micro-Newton resolution and the micro manipulation system operating micrometer level of the displacement. Another one is to build suitable strategy of the noise rejection for the target application.

RQ2. Is there any micro-tensile testing machine or testers usable for target application of this thesis work?

Based on the survey in Section 2.2.3, the micro-tensile testing machine and testers are classified into the micro-tensile testing machine using the load cell [20, 25-34], AFM with the nano-indenter [18] and the special cantilever [32][33], and the micro-tensile testers created for target applications [23, 37-41]. Each category is also divided depending on types of the specimens, e.g. the thin film, fiber, others such as polymide substrate and muscle cell, and measured mechanical properties, e.g. the tensile stiffness and bending stiffness of the specimen. As in this thesis, it uses the existing open loop microrobotic platform to measure the tensile stiffness of the micro-scale fibers, it may be considerable to use the Hopkinson Bar based tensile testing machines for this application. This is because they measured the tensile stiffiness for the fiber specimen, despite their drawbacks mentioned in Section 2.2.4. The tensile tester in [23] is the reasonable candidate in a way that it used the microrobtic platform to measure the mechanical properties of the IPF. However, since the microrobotic platform in [23] was to measure bending stiffness of the IPF while the target application of this thesis work is to measure the tensile stiffness, they are still different application areas. They also have different test environments, e.g. the specimen, force sensor and testing platform.

It is still challenging to find suitable method applicable for the thesis work as none of studies had clearly explained the way to apply the force feedback control for the micro-

tensile testing of the micro-scale fibrous materials. Moreover, since the test environment such as the testing platform, specimen and target mechanical property to be measured are different depending on their applications, it is not possible to find turn-key solution. Therefore, the author has focused to describe novel way to implement the force feedback controller for the tensile testing of the micro-scale fibrous materials in this thesis work. It is the meaningful because it is first trial to apply the force feedback control mechanism to the material testing applications.

3 RESEARCH METHODOLOGY AND MATERIALS

This chapter provides the reader with details of the research method and material employed in this thesis work. Specifically, Section 3.1 offers the hardware architecture of the microrobotic platform used to execute micropositioning and force measurement task. It also includes the explanation of the four different functions of the microrobotic platform. Section 3.2 illustrates the requirement and the implementation of the computer model for the tensile testing simulation. To obtain usable controller parameters, it uses the conventional rule based tuning methods such as the Ziegler-Nichols tuning, Pessen Integral of Absolute Error (PIAE), Some overshoot rule (SO-OV) and No overshoot rule (NO-OV), and Simulink PID tuner. Details of the controller tuning are described in section 3.3.

3.1 Microrobotic Platform

In this thesis work, the force feedback control is applied to the existing microrobotic platform. Before going into the detail on the implementation of the force feedback control, it is necessary to understand the structure and the technical specifications of the microrobotic platform and they are explained in this section.

The microrobotic platform is used for tensile testing of fibers as follows. First, a fiber to be measured is placed manually between two clamps. The clamps are closed using mounting screws. After closing the clamps, the tensile test is performed by moving one of the clamp with a motor and measuring the generated force using a force sensor. The fiber can be image during the measurement.

The microrobotic platform consists of several sub-units and each of them have different function in the tensile testing process such as the micromanipulation (clamping of the fiber, moving the clamp), force sensing, visualization (magnification, illumination and imaging), and control (data acquisition, manipulator control, visualization control, force control, user-interface) as illustrated Figure 14.

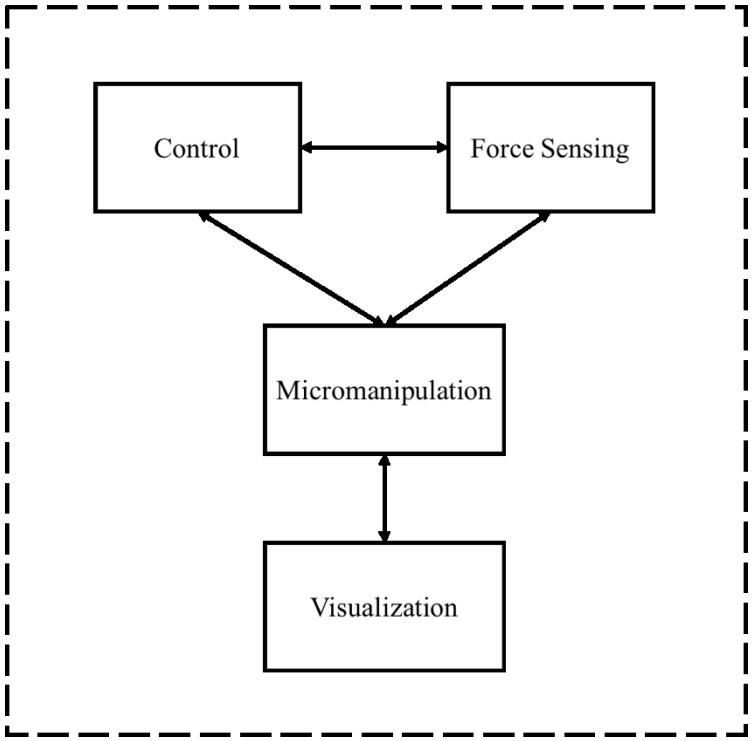

Figure 14. *Main functions and sub-unit interaction of microrobotic platform*

3.1.1 Micromanipulation

The micromanipulation function performs micropositioning to move toward the desired position within the working space of the clamp. For the robust and accurate micropositioning during the tensile test, a M.111.1 DG Micro-translation stage from Physik Instrumente, GmbH & Co, Karlsruhe, Germany is chosen. Please see Figure 15.

Figure 15. *Product view of M-111.1 DG, 1 is base body, 2 is moving platform, 3 is cable of the connection to the motor controller and 4 is DC gear motor [42].*

As the leadscrew-driven translation stage, the M.111.1 DG Micro-translation stage has 15 mm travel range and 1.5 mm/s maximum velocity. The maximum carrying loads is

0.4 kg. The precision linear bearings equipped guarantee a guidance accuracy of $<0.5\ \mu m$. A small DC gear motor (DG) drives the stage through a backlash-compensated screw and a nut system with a gearhead. A rotary encoder is also installed with the DG in order to achieve the design resolution of 0.007 μm per the impulse. It also supports the minute increments of 50 nm at 1.5 mm/s of the speed by the combination of low adhesion and friction with high resolution encoder [42]. For the interface between a computer and M.111.1 DG Micro-translation stage, C-863 Mercury™ DC motor controller from Physik Instrumente, GmbH & Co, Karlsruhe, Germany is utilized. It is the PID servo controller and has the trajectory profile mode of the trapezoidal point-to-point. It also supports to communicate with the host computer via a single RS-232 or USB port [43].

3.1.2 Force Sensing

During the experiments, this function measures the magnitude of the force to pull the fiber to be tested in milli-newton range. When the force is applied to an object, it triggers changes on the position and the structure of the object. Once the interaction between the force and the change of the object structure is known, it is able to estimate the mechanical property of the fiber.

In a typical experiment the glass fiber is fixed between the two clamps. The tensile force is measured while one clamp starts to pull the glass fiber. For the force measurement, FUTEK LPM200 Panel Mount Load cell, FUTEK Advanced Sensor Technology, Irvane, CA, USA is used. Please see Figure 16. Specifically, a FSH03398 model in LPM200 series is chosen as it offers low capacity range, 100 g with 1000 % overhead protection and the high accuracy under the operating temperature from -19℃ to 105℃ [45].

Figure 16. *Product view of FUTEK LPM200 Panel Mount Load cell [45]*

3.1.3 Control

The control function encompasses three sub-functions as below.

1) Micromanipulation control: controlling micropositioning.

2) Visualization control: adjusting zoom and fine focus.
3) Force feedback control: producing sensible force feedback to control system.

All control sub-functions are connected with human operator via the sub-function of the user interface. Specifically, PImikromove from Physik Instrumente, GmbH & Co is used to control the micropositioning of the M.111.1 DG Micro-translation stage. Navitar controller and MATLAB, The MathWorks Inc. are employed for the visualization control and force feedback control, respectively.

3.1.4 Visualization

The visualization function consists of following sub-functions.

1) Imaging: obtaining visual information.
2) Magnification: magnifying the object to be characterized.

For the function operation, Navitar motorized optics is chosen. It performs 12x zoom with 2x extending tube and 2x magnification lens. Navitar's control software is used for the sub-functions such as the imaging and magnification.

3.2 Numerical Model for Tensile Test Simulation

This section provides details of the mathematical models of the M-111.1 DG Micro-translation stage and the glass fiber. The computer model is created by that mathematical models for the tensile testing simulation. Simulink, The MathWorks Inc., Natick, MA is employed to build the computer model under 50 Hz of the sampling frequency and 50 ms of the delay is applied to the input. The force feedback control mechanism by the PI and PID controllers is applied to the computer model. The point to point motion profile of the force input is generated by the signal generator and the output is decided depending on the level of the deflection by the linear mathematical model of the glass fiber.

Section 3.2.1 presents the mechanism of the force controllers. Section 3.2.2 is about the general idea of the point to point motion profile for the force input. Section 3.2.3 and 3.2.4 describe the model developments for the M-111.1 DG Micro-translation stage and the glass fiber, respectively.

3.2.1 Force Controllers

The main purpose of the tensile testing simulation is to find a usable set of controller parameters such as proportional gain P, integral gain I and derivative gain D. With the computer model of the M-111.1 DG Micro-translation stage, it is able to achieve this purpose. During the simulation, the force feedback controller is utilized. The computer model is created via the Simulink and the computer model consists of the signal generator, the PI and PID controllers, the models of the M-111.1 DG Micro-translation stage and the glass fiber, etc. Figure 17 illustrates the block diagram of the simplified model of the force feedback control.

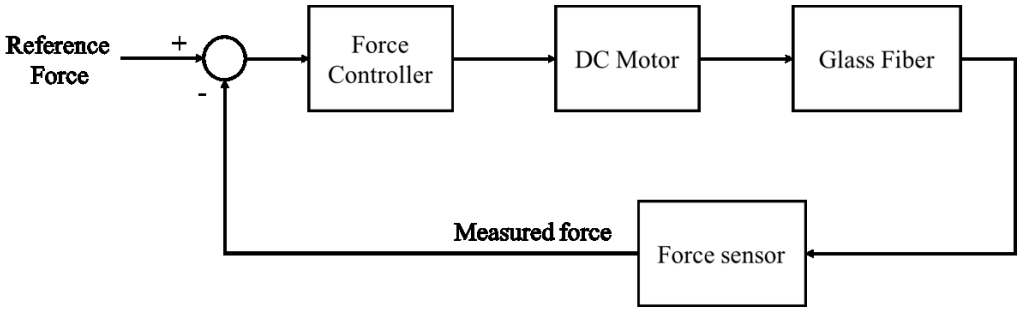

Figure 17. *Block diagram of simplified model of force feedback control*

3.2.2 Signal Generator

The signal generator produces the point to point motion profile of the force input to the computer model of the microrobotic platform. Once the motion profile of the reference force is applied as the input, the computer model can specify the required velocity and position of the M-111.1 DG Micro-translation stage. Then, it linearly accelerates and decelerates to arrive in the reference force. Figure 18 shows an example of the point to point motion profile of the force input.

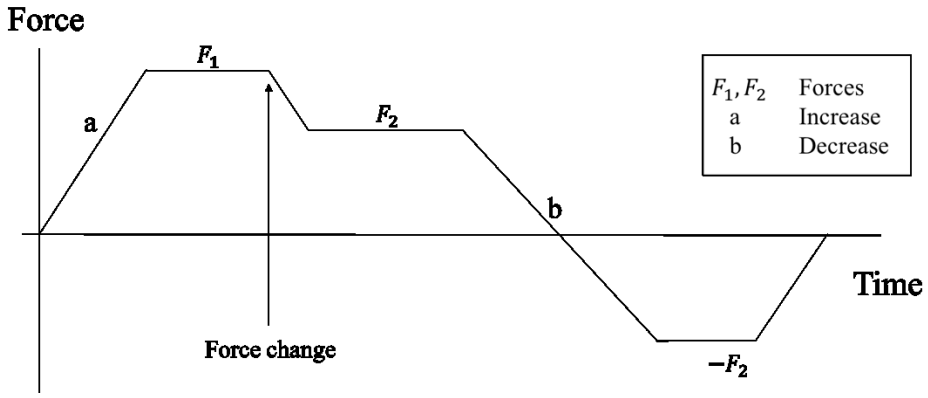

Figure 18. *Example of force curve in the point to point motion profile*

3.2.3 DC Gear Motor with Leadscrew

Mathematical model

The details of the development of the mathematical model of the M-111.1 DG Micro-translation stage are explained, which is necessary task before building its computer model. The M-111.1 DG Micro-translation stage is driven by a small DG and its rotary motion is directly transferred to the rotation of the leadscrew. In this sense, it can be modelled as the leadscrew driver. Figure 19 shows the block diagram of the M-111.1 DG Micro-translation stage.

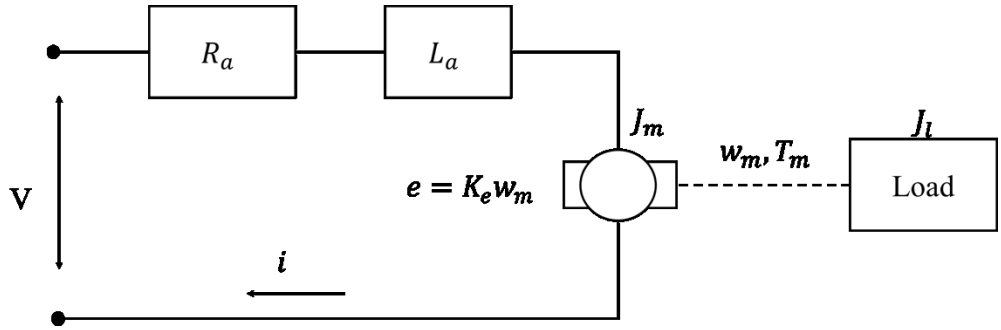

Figure 19. *Block diagram of M-111.1 DG Micro-translation stage*

The leadscrew is directly coupled to the motor shaft with a pitch of p. Weight of the leadscrew is W_{ls} and a carriage with the load is denoted as W. Translational movement of the carriage is performed via the rotation of the screw translated from the rotary movement of the motor shaft. In this regard, this system can be described by the differential equation as below [44].

$$V = L_a i' + R_a i + e \tag{16}$$
$$e = K_e \cdot w_m \tag{17}$$

According to the Kirchhoff's voltage law, Equation 16 can be defined. where V, i, i', L_a and R_a are the applied voltage, the current of motor, the derivative of the motor current, the motor inductance and the resistance, respectively. In Equation 17, e, K_e and w_m are the back Electro-Motive Force (EMF), the back EMF constant and the angular velocity of motor shaft, respectively [44]. The torque calculation of the DG drive with some adjustments can be defined in Equation 18.

$$T_m = T_a + T_f + T_l \tag{18}$$

Where T_m, T_a, T_f and T_l are the motor torque, the acceleration torque, friction torque and load torque, respectively. In the DG, as the motor torque is the proportional to the motor current i with the motor torque constant K_t, the motor torque can be shown as follows [44].

$$T_m = K_t \cdot i \tag{19}$$

As the friction torque is proportional to the angular velocity of the motor with a proportional factor B, it is described in Equation 20 [44].

$$T_f = B \cdot w_m \tag{20}$$

The load torque can be expressed as following equation by the load of the leadscrew reflected to the DG [44].

$$T_l = \frac{W}{2\pi p} \tag{21}$$

Where W is the weight of the carriage with the load and p is the pitch of the motor shaft. In order to calculate the acceleration torque T_a, it is necessary to estimate the total inertia of whole system, J. It can be defined as $J = J_m + J_l + J_{ls}$, where J_m, J_l and J_{ls} are

the motor inertia, the leadscrew inertia and the load inertia, respectively [44]. The leadscrew inertia is estimated if some parameters of the leadscrew such as the radius R_{ls} and the weight W_{ls} or the radius R_{ls}, the length L_{ls} and the density ρ_{ls} are known with the gravitational constant g [44].

$$J_{ls} \approx \frac{W_{ls}{R_{ls}}^2}{2g} \approx \frac{\pi L_{ls}\,\rho_{ls}\,{R_{ls}}^4}{2g} \tag{22}$$

The load inertia is described by the following equation as it has to be reflected back to the DG [44].

$$J_l = \frac{W}{g}\frac{1}{(2\pi p)^2} \tag{23}$$

Then, the acceleration torque T_a can be expressed in Equation 24 [44].

$$T_a = J\dot{w}_m = (J_m + J_l + J_{ls})\dot{w}_m \tag{24}$$

Equation 16 and 18 above can be illustrated again as [44].

$$L_a i' = V - R_a i - K_e w_m \tag{25}$$

$$(J_m + J_l + J_{ls})w_m' = K_t i - B w_m - \frac{W}{2\pi p} \tag{26}$$

During the operation of the leadscrew driver, the rotational movement of the motor shaft is transformed to the translational movement by the screw. The leadscrew driver has the pitch p of 0.4 $mm/revolution$ [42]. Thus, the transformation from the angular velocity to translational velocity is performed by multiplying with $\frac{p}{2\pi}$, which is utilized in the computer model in the Simulink [44].

In this linear model of the leadscrew driver, some factor such as the friction force between the leadscrew and the carriage, and efficiency of the leadscrew have been neglected. Moreover, the system nonlinearities such as the backlash or the dead zone of the DG are not considered in this model.

Computer model

During the tensile testing, the angular rotation of the armature of the DG is transformed into the translational movement of the leadscrew carriage. This movement triggers the pulling force to deflect the glass fiber. Figure 20 shows the computer model of the M-111.1 DG Micro-translation stage. It is created by Equation 25 and 26, including additional nonlinear elements such as the dead zone, the velocity dependent friction and the backlash [44].

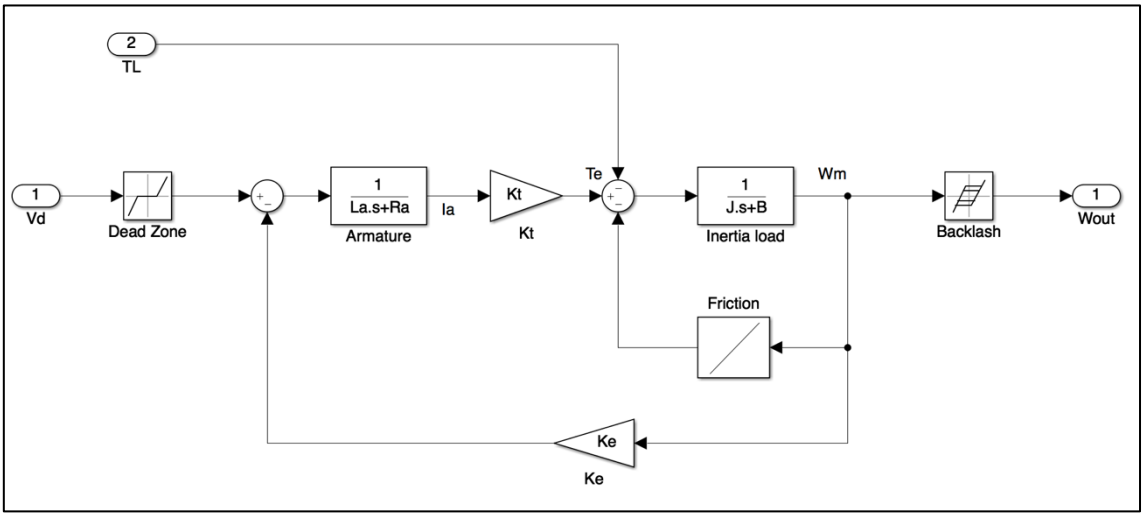

Figure 20. *Nonlinear computer model of the M-111.1 DG Micro-translation*

Per the nonlinear elements, the dead zone is normally triggered when the system stays without any motion, i.e. when the armature voltage of the DG is around zero [44]. It causes the state, where the system does not operate immediately against the input signal because it is under the rest state [44]. The system only starts responding to move when the driving force is higher than the certain level. The parameters of the start of the dead zone and the end of the dead zone are defined as the lower limit $V_{d\ -}$ and the upper limit $V_{d\ +}$, respectively [44].

$$deadzone\ (V_d) = \begin{cases} (V_d - V_{d\ +}), V_d \geq V_{d\ +} \\ (V_d - V_{d\ -}), V_d \leq V_{d\ -} \\ 0 \quad , otherwise \end{cases} \tag{27}$$

The velocity dependent friction is assumed as following form [44]:

$$friction\ (w) = B \cdot w_m \tag{28}$$

The backlash is applied to the system as Equation 29 [44]. In general, the backlash is implemented to the system where the change in the input equally changes in the output. However, the change in the input does not affect the output when the input changes direction [44].

$$backlash\ (w_m) = \int w'_{out} dt \tag{29}$$

$$w'_{out} = \begin{cases} w'_m\ , \ |w_{out} - w_m| = D_{ead} \\ and\ w'_m\ (w_m - w_{out}) > 0 \\ 0 \quad , \quad otherwise \end{cases}$$

Where D_{ead} and w_{out} denote the deadband which is the amount of side-to-side play in the system and output of the backlash block, respectively [44].

Table 3 represents specific parameters of the M-111.1 DG Micro-translation stage used in the computer models. They are obtained directly by its technical documentation [46] and supplier, i.e. Physik Instrumente.

Table 3. *Specific parameters of the M-111.1 DG Micro-translation*

Parameters	Symbols	Values
Motor inductance	L_a	$0.42\ mH$
Motor resistance	R_a	$19.8\ \Omega$
Back EMF constant	K_e	$74.4\ mVs$
Angular velocity of motor shaft	w_m	$124.103\ rad/sec$
Motor torque constant	K_t	$11.5\ mNm/A$
Motor inertia	J_m	$0.56\ g \cdot cm^2$
Pitch of motor shaft	p	$0.4\ mm$
Gravitational constant	g	$9.8\ m/sec^2$
Radius of leadscrew	R_{ls}	$3\ mm$
Weight of leadscrew	W_{ls}	$11g$
length of leadscrew	L_{ls}	$64\ mm$
Density of leadscrew	ρ_{ls}	$0.078\ g/mm^2$
Proportional factor	B	$0.645\ Nm/(rad/sec)$
Deadzone upper limit	V_{d+}	$0.2V$
Deadzone lower limit	V_{d-}	$-0.2V$

3.2.4 Fiber Model

Mathematical / Analytical model

One of the technical requirement of the computer model is to estimate the force magnitude as it is useful when user chooses a suitable micro force sensor used in the real experiment [23]. For this work, following mathematical model of the glass fiber is used based on the Hooke's law under assumption that it has linear mechanical behavior.

First of all, the fiber tensile stress (σ) and strain (ε) are shown in Equation 30 and 31. Based on the stress and strain, Young's modulus (E) is defined in Equation 32.

$$\sigma = \frac{F}{A} \tag{30}$$

$$\varepsilon = \frac{\Delta l}{L} \tag{31}$$

$$E = \frac{\sigma}{\varepsilon} \tag{32}$$

Where F is the pulling force and A is the cross-sectional area of the glass fiber. L and Δl are the initial length of the glass fiber and the change in length during the tensile testing, respectively. Based on Equation 32, the glass fiber model is defined as below.

$$F = \frac{A \cdot E}{L} \Delta l \tag{33}$$

Equation 33 establishes a linear relationship between the pulling force and the deformation on the glass fiber. The computer model of the glass fiber is created by Equation 33. Table 4 shows the parameters used in the computer model of the glass fiber.

Table 4. *Specific parameters of glass fiber*

Parameters	Symbols	Values
Young's modulus of glass fiber	E	$80\ GPa$
Initial length of glass fiber	L	$12\ mm$
Radius of glass fiber	r	$10\ \mu m$

3.3 PI and PID Controller Tuning

In the computer model of the microrobotic platform, the PI and PID controllers are employed. Equation 34 and 35 provide the mathematical forms of the PI and PID controllers, respectively.

$$u(t) = K_p e(t) + K_i \int_0^t e(\tau) d\tau \tag{34}$$

$$u(t) = K_p e(t) + K_i \int_0^t e(\tau) d\tau + K_d \frac{de(t)}{dt} \tag{35}$$

Where K_p, K_i, and K_d mean the coefficients for the proportional, integral and derivative terms respectively. $u(t)$ is the correction from the error $e(t)$. K_i and K_d can be replaced with $\frac{K_p}{T_i}$ and $K_p T_d$, respectively. T_i denotes the integration time and T_d indicates the derivative time.

In order to obtain usable controller parameters, two approaches are used. The first approach is to use the conventional rule based tuning methods such as the Ziegler Nichols, the Pessen Integral of Absolute Error (PIAE), Some overshoot rule (SO-OV) and No overshoot rule (NO-OV) as described in Section 3.3.1 and Section 3.3.2. The second approach is to employ the Simulink PID tuner which is presented in Section 3.3.3.

3.3.1 Ziegler Nichols Tuning Method

The Ziegler Nichols tuning method was developed by J. Ziegler and N. Nichols which is the well-known tuning method for the PID controller. For controller tuning, this method is utilized to obtain the PI and PID controller parameters. The specific procedures of the Ziegler Nichols tuning method are as following [47][48].

1) Tune the controller to P only mode, i.e. set the integral gain I and the derivative gain D to zero.
2) Increase the proportional gain, K_p from zero until ultimate gain K_u is reached, at which the output of the control loop has stable and sustained oscillations.
3) Measure the period of the oscillation of the response to obtain the oscillation period T_u.
4) Apply K_u and T_u to the Ziegler-Nichols tuning chart in Table 5 to obtain the P, I and D gains depending on which type of controller is desired.

Table 5. *Ziegler-Nichols Tuning Chart [48]*

Control Type	K_p	T_i ($Intergal\ time$)	T_d (Derivative time)
P	$0.5\ K_u$	-	-
PI	$0.45\ K_u$	$T_u/1.2$	-
PID	$0.6\ K_u$	$T_u/2$	$T_u/8$

3.3.2 Other Tuning Rules

Besides the Ziegler-Nichols tuning method, other rule-based tuning methods such as the PIAE, the SO-OV and the NO-OV are performed in order to find usable controller parameters. Details on each method are described as below.

Pessen Integral of Absolute Error (PIAE)

The PIAE was developed for interacting the PID controller without the ideal PID relationship [48].

$$U(s) = K_p\left(1 + \frac{1}{T_i s} + T_d s\right) E(s) \tag{33}$$

Where $U(s)$ and $E(s)$ denotes the actuation and the error signal, respectively. The Pessen suggested IAE formula for the certain controller model processing with the time delay such as a first order lag plug delay (FOLPD) model [48]. This model was able to estimate the frequency response of the system based on the knowledge of frequency response for the process such as the time delay, the FOLPD model was given by

$$G(s) = \frac{K_p}{1+sT} \cdot e^{-sD_l} \tag{34}$$

Where T and D_l mean the time constant and the delay time, respectively [48].

Some Overshoot Rule (SO-OV)

The formula of the SO-OV was obtained by simply modifying the Ziegler-Nichols tuning rule. This rule was used to decrease the level of the overshoot against changes of the set point [48].

No Overshoot Rule (NO-OV)

Main purpose of the formula of the NO-OV was to make no overshoot against the changes of the set point [48].

Table 6 shows tuning charts for aforementioned tuning rules to obtain required controller parameters such as K_p and T_u mentioned in section 3.3.1.

Table 6. *Summary of PIAE, SO-OV and NO-OV tuning rules [48]*

Tuning Rule	Required	Controller Type	Controller Parameters
PIAE	K_u, T_u	*PID*	$K_p = 0.7\ K_u,\ T_i = 0.4\ T_u,\ T_d = 0.15\ T_u$

SO-OV	K_u, T_u	*PID*	$K_p = 0.33\,K_u,\ T_i = 0.5\,T_u,\ T_d = 0.33\,T_u$
NO-OV	K_u, T_u	*PID*	$K_p = 0.2\,K_u,\ T_i = 0.5\,T_u,\ T_d = 0.33\,T_u$

3.3.3 Simulink PID Tuner

In the Simulink, the tuning feature of the PI and PID controllers is utilized to gain the controller parameters. This PID tuner offers the single-loop PID tuning method for the PID controller blocks to tune the controller parameters in a short time. The tuning procedures is described as below [49].

1) Run the Simulink PID Tuner. When starting to run, the Simulink PID tuner automatically designs an initial controller from the Simulink model.
2) Tune the controller by manually adjusting design criteria via the PID tuner to find the PID controller parameters to stabilize the system.
3) Export the parameters for the designed controller and check the controller performance via the Simulink.

4 EXPERIMENT AND RESULTS

This chapter explain the details of the experiment such as the testing procedure and test results. Section 4.1 indicates the simulation result by the computer model of microrobotic platform where the force feedback control system is applied. Section 4.2 deals with discussion for the simulation result of the computer models. Section 4.3 and Section 4.4 describe the experiment procedure and test results of the open loop system and the force feedback control system applied to the microrobotic platform, respectively. Lastly, the discussion of the experiment result of the real microrobotic platform is illustrated in Section 4.5.

4.1 Simulation Result of Computer Models

To find controller parameters using the selected tuning methods and perform step-response simulations to compare the different tuning methods, the tensile testing simulation is executed. This section offers the implementation of the microrobotic platform and the simulation result on the step response of the computer model with the force feedback control described in Section 3.2. In order to find usable PI and PID controller parameters, the different rules based tuning methods such as the Ziegler Nichols, PIAE, SO-OV and NO-OV, and Simulink PID tuner are utilized by following tuning processes.

4.1.1 Implementation of the Microrobotic Platform

The design of the microrobotic platform is shown in Figure 21 and it is organized following components.

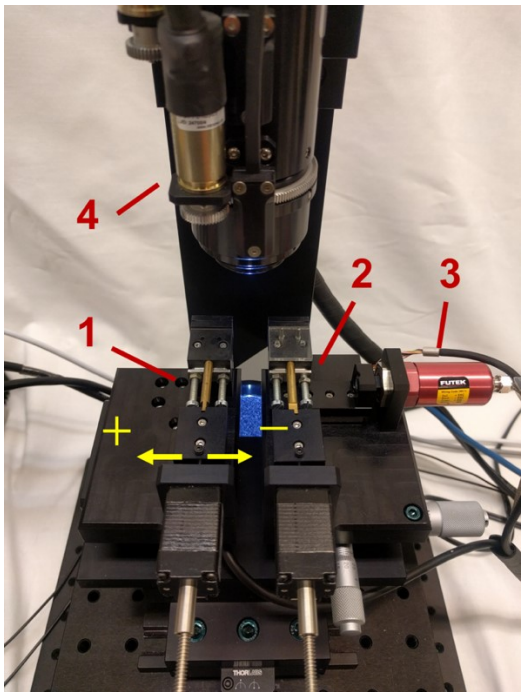

Figure 21. *Design of the Microrobotic platform*

1) The first clamp fixed on M.111.1 DG Micro-translation stage. + and – coloured by yellow in Figure 21 means the DG movement toward to left and right directions, respectively.
2) The second clamp connected with the force sensor.
3) Force sensor, FSH03398 of FUTEK Advanced Sensor Technology.
4) Navitar motorized optics, Blackfly S BFS-U3-32S4M.

Regarding the operation principal of the existing microrobotic platform, it basically operates to grasp the micro-scale fibrous materials by two clamps. One clamp is connected to a velocity controlled M.111.1 DG Micro-translation stage, Physik Instrumente GmbH & Co, Karlsruhe, Germany and the other clamp is directly connected to a force sensor of FUTEK LPM200 Panel Mount Load cell, FUTEK Advanced Sensor Technology, Irvane, CA, USA. Therefore, once the clamp moved by the DG starts pulling the fiber, the pulling force is measured by the force sensor on another clamp as the open loop system during the tensile testing.

4.1.2 Behavior of DC Gear Motor with Leadscrew

The linear computer model of the M.111.1 DG Micro-translation stage excluding the the dead zone, the velocity dependent friction and the backlash is simulated by different voltage inputs from 2 V to 12 V to investigate its operational behavior. The simulation result is shown in Figure 22. During the simulation, 1 sec is used as the step time for producing the voltage inputs to the M.111.1 DG Micro-translation stage.

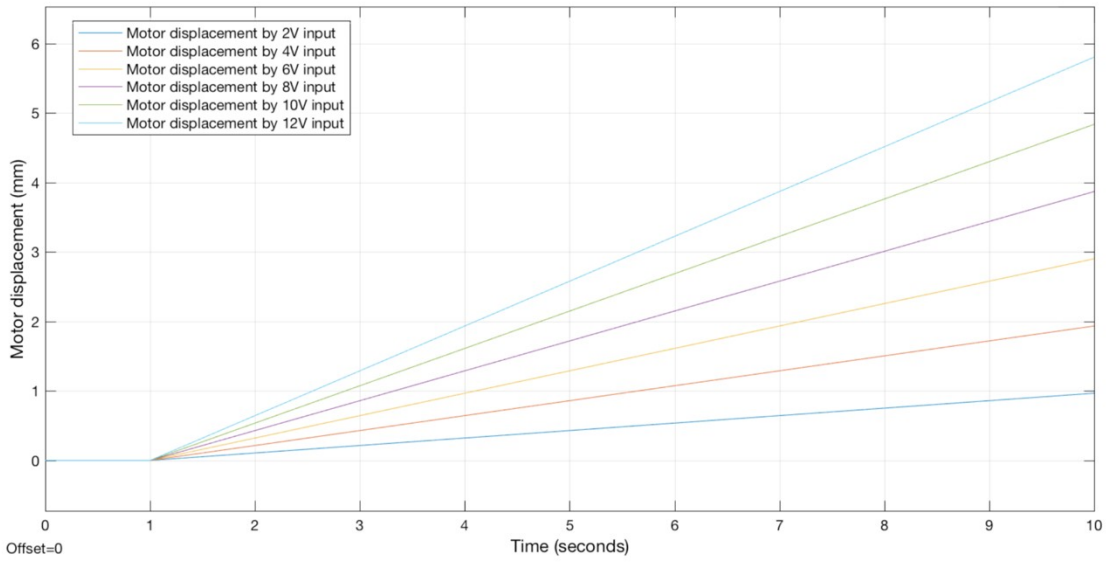

***Figure 22**. Simulation result of M.111.1 DG Micro-translation stage*

The simulation results in Figure 22 indicate that the outputs of the motor displacement are increased in proportion to the increment of the input voltage and vice versa.

4.1.3 Tuning Process of Rules Based Tuning Methods

In order to find usable controller parameters, different rule based tuning methods are used. This section offers the tuning process and results.

1) Obtain K_u and T_u by following the tuning procedure in Section 3.3.1. The parameters, 237.6 and 0.239 are obtained for K_u and T_u, respectively.
2) Apply obtained K_u and T_u to the tuning charts of Table 5 and 6 in order to find K_p, T_i and T_d. Table 7 shows the controller parameters gained from the tuning charts of Table 5 and 6.

Table 7. *Result of controller parameters for rule based tuning methods*

Tuning Rule	Controller Type	Controller Parameters
Ziegler Nichols	*PI*	$K_p = 106.92,\ T_i = 0.199$
Ziegler Nichols	*PID*	$K_p = 142.56,\ T_i = 0.12,\ T_d = 0.03$
PIAE	*PID*	$K_p = 166.32,\ T_i = 0.096,\ T_d = 0.036$
SO-OV	*PID*	$K_p = 78.408,\ T_i = 0.12,\ T_d = 0.079$
NO-OV	*PID*	$K_p = 47.52,\ T_i = 0.12,\ T_d = 0.079$

3) Apply obtained K_p, T_i and T_d to the computer model of each controller.

4.1.4 Tuning Process of Simulink PID tuner

To figure out usable controller parameters, the Simulink PID tuner is used. This section provides the tuning process and result.

1) Find usable parameters of the controller by using the Simulink PID tuner as mentioned in Section 3.3.3. The parameters, 35.82 and 41.35 are obtained for P and I, respectively.
2) Apply obtained P and I parameters to the computer model of the controller.

4.1.5 Step Response of Force Controller Tuned by Tuning Rules and Simulink PID Tuner

For the tensile testing simulation, 200 mN step function goes through the computer model as the input signal F_{in} with 50 ms time delay to the input. 50 Hz sampling frequency is utilized. The PID and PI controller parameters obtained using different tuning methods in Section 4.1.2 and 4.1.3 are compared in this section. For the glass fiber model, the Young's modulus (80 GPa), the radius of the glass fiber (10 μm) and the length of the glass fiber (12 mm) are used based on Equation 30. Any nonlinear elements such as the disturbance is not considered in this computer model. Figure 23 represents the step response, i.e. the measured force F_m via the controllers tuned by different tuning methods against the input step function.

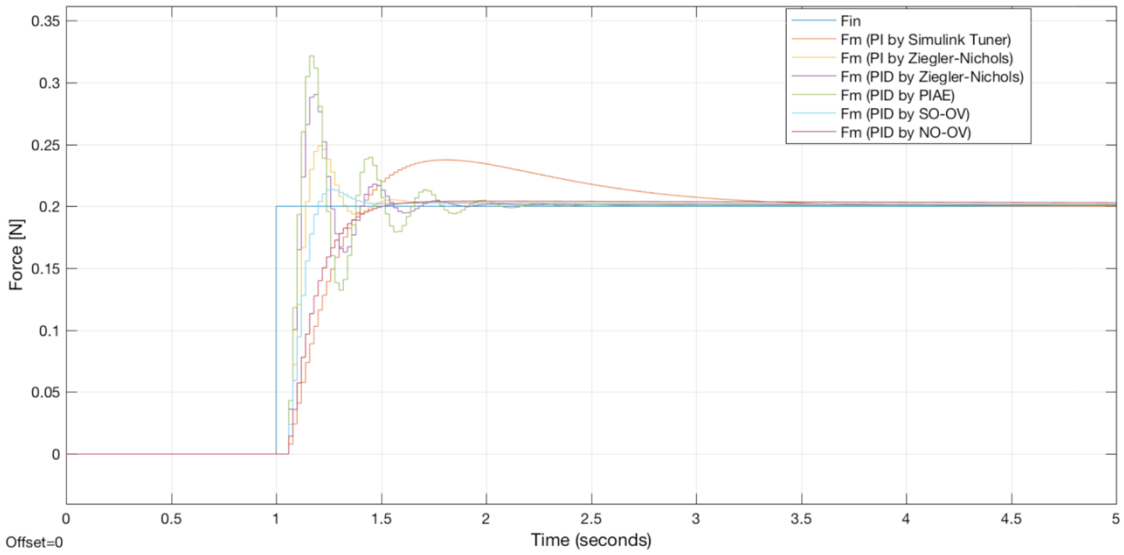

Figure 23. *Step responses of computer model of force control system tuned by rule based tuning method and Simulink PID tuner*

The characteristics such as the rise time, overshoot and undershoot of each step response by the different tuning methods are shown in Table 8 and are directly measured by the scope bilevel measurement panel in Simulink. Each of characteristics has following meaning.

- Rise time: Average time rising from the lower reference level to the upper reference level.
- Overshoot: Average of maximum difference of the area in each rising transition.
- Undershoot: Average of minimum difference of the area in each rising transition.

Table 8. *Step responses for linear computer model tuned by different tuning methods*

Tuning method	Controller Type	Rise time	Overshoot	Undershoot
Simulink Tuner	PI	259.349 ms	18.452 %	0.282 %
Ziegler Nichols	PI	70.691 ms	22.840 %	3.384 %
Ziegler Nichols	PID	53.823 ms	44.203 %	1.926 %
PIAE	PID	46.725 ms	60.484 %	2.571 %
SO-OV	PID	107.480 ms	5.851 %	-0.110 %
NO-OV	PID	256.768 ms	0.505 %	1.958 %

The step response by the computer model with the nonlinear elements such as the dead zone, the backlash and the friction mentioned in Section 3.2.3 is shown in Figure 24.

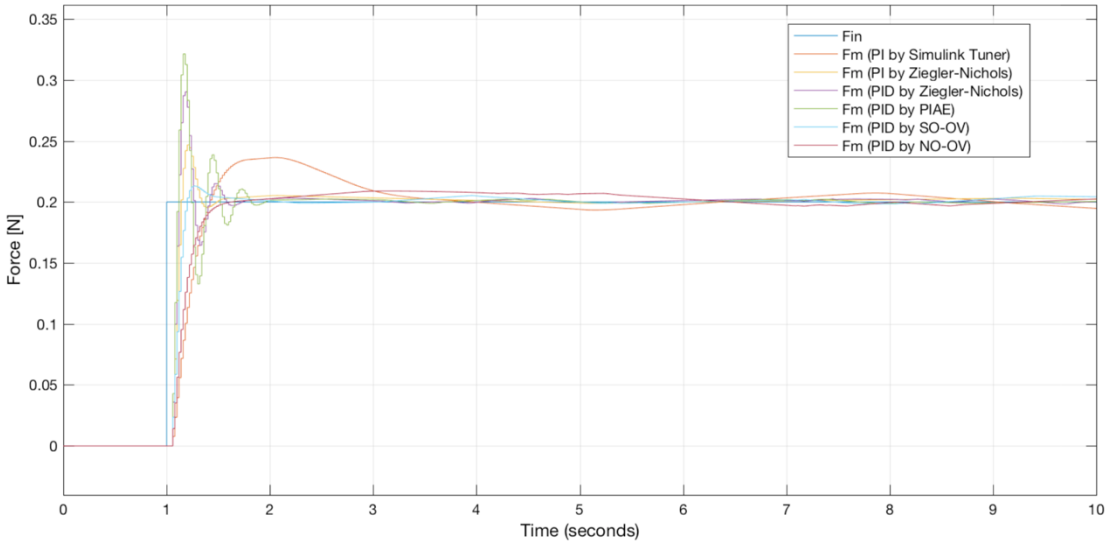

Figure 24. *Step responses of tuned computer model of force control system tuned by rule with nonlinear elements*

The characteristics of each step response for the nonlinear computer model according to the different tuning method are shown in Table 9.

Table 9. *Step responses for nonlinear computer model tuned by different tuning methods*

Tuning method	Controller Type	Rise time	Overshoot	Undershoot
Simulink Tuner	PI	259.804 ms	19.880 %	0.325 %
Ziegler Nichols	PI	70.877 ms	22.840 %	1.242 %
Ziegler Nichols	PID	54.179 ms	44.203 %	0.308 %
PIAE	PID	46.963 ms	60.484 %	0.832 %
SO-OV	PID	105.800 ms	6.989 %	-1.996 %
NO-OV	PID	298.042 ms	0.492 %	1.953 %

During the tensile testing of the micro-scale fibrous materials, the high overshoot of the pulling force, can generate to break the fibrous materials. In this regard, the PID controller tuned by the NO-OV is the most reasonable for this application because it provides the lowest overshoot compared with those of others tuned by other tuning methods in Table 8 and Table 9.

4.1.6 Behavior of Force Controller Tuned by No Overshoot Rule

In order to investigate the behavior of the PID controller tuned by NO-OV in the nonlinear computer model of the microrobotic platform, the simulation results by different force signals as the target inputs are presented. Specifically, Figure 25 shows the different step responses against the step functions of different force inputs from 0.2 N to 1 N.

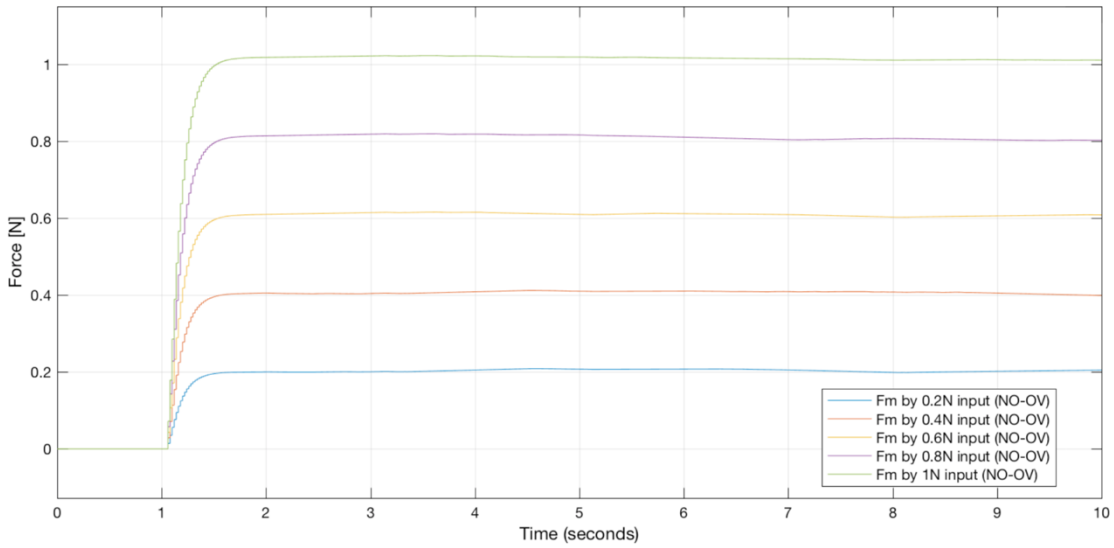

Figure 25. *Step responses of PID controller tuned by NO-OV*

The control result for a ramp type input signal is represented in Figure 26.

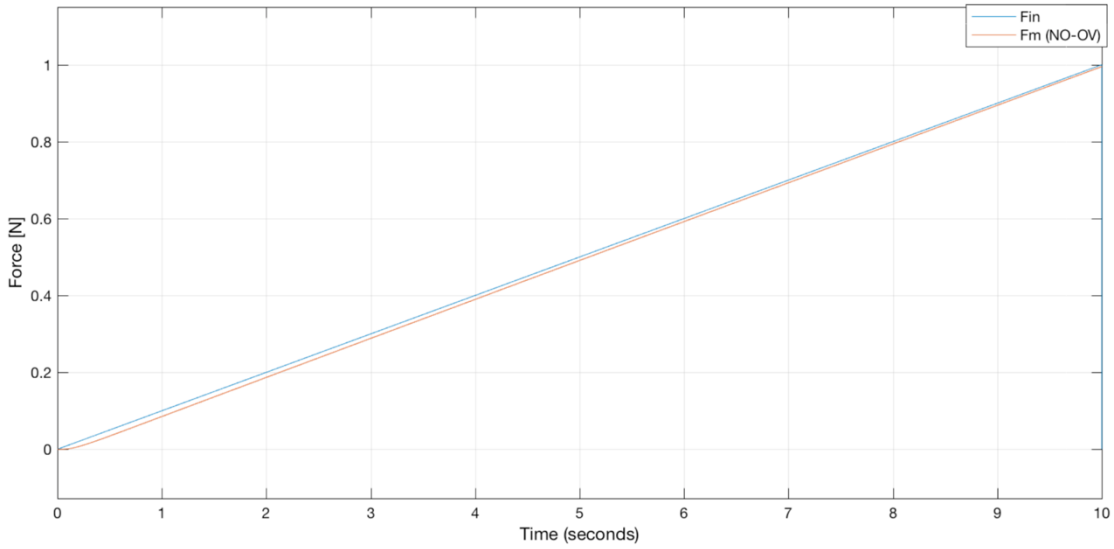

Figure 26. *Response of PID controller tuned by NO-OV to a ramp signal.*

All of the results in Figure 25 and 26 indicate that the output signals have $\pm$ 1 % overshoot approximately.

4.2 Discussion

The main target for the tuning process is to find the usable controller parameters and Table 8 and Table 9 represents the results of the step response by the linear and nonlinear computer models tuned by different tuning methods, respectively. Specifically, the step response obtained with the Simulink tuner shows the slow rise time with good level of overshoot and the lowest undershoot. The fastest rise time is achieved by the PIAE rule but it has the highest overshoot and undershoot compared with those of other rules. The step response with Ziegler Nichols rules exhibits the middle level of the rise time,

overshoot and undershoot. Also, the SO-OV and NO-OV rules show expected results as their purposes. The SO-OV rule was developed to decrease the overshoot and its result also shows the lower overshoot and undershoot than those of the Ziegler Nichols and PIAE rules with fast rise time. The lowest overshoot with the slowest rise time is detected from the step response with the NO-OV rule as this rule is to make no overshoot. These results are visible in both Table 8 and 9 regardless of whether it is the linear or nonlinear computer models.

Based on the simulation results by the different tuning methods, it is noticeable that the controller parameters obtained by the NO-OV rule is the reasonable for the tensile testing of the micro-scale fibrous materials because it always shows low overshoots ($\pm$ 1 %) against the different input signals as presented in Figure 25 and 26. The low overshoot is important in material testing applications as a too large over-shoot might lead to a breakage of the fiber.

As the rule based tuning methods reply on proportional measurement to estimate integral (I) and derivative (D) controllers, it is difficult to use for I, D or proportional derivative (PD) controllers. The Simulink tuner can be alternative solution for this case. However, controller parameters obtained by both the rule based tuning methods and the Simulink tuner are not accurate for different platform models as they are tuned for one particular platform model. Thus, it still requires time consuming for the user to find usable controller parameters for other platform models. Nevertheless, as those tuning methods are very easy to implement and robust, they are still popular. The developed simulation model can be also used with more complicated fibers such as cellulose fibers if the fiber model is updated corresponding the behaviour of the fiber.

4.3 Experiment and Result of Open Loop System

This section provides the experiment and the result of the open loop microrobotic platform to understand the current behavior and the limitation. For the tensile testing, the real microrobotic platform mentioned in Section 4.1.1 is utilized with Jushi E6 CR glass fiber of 16 μm to 20 μm in the diameter and around 32 mm in length. Its Young's modulus from the manufacturer is 80 GPa. PImikromove and Navitar controller are used for the micromanipulation and visualization controls, respectively as mentioned in Section 3.1.3 and 3.1.4. The experiment is performed by following procedures.

4.3.1 Experiment Procedures of Open Loop System

1) Prepare the single Jushi E6 CR glass fiber and place it on two clamps.
2) Set 10 mm as the initial position of the M.111.1 DG Micro-translation stage and the constant velocity to 0.016 mm/s by the PImikromove.
3) Fix the glass fiber by the clamps. The clamped length of the fiber is 32 mm which is the distance between two clamps holding each end of the fiber.
4) Run the tensile testing by the PImikromove and monitor the time graph of the measured voltage by NI LabVIEW SignalExpress.

5) Increase 0.1 mm of the displacement of the M.111.1 DG Micro-translation stage under the certain time period until it reaches to the moment when the glass fiber is broken by the PImikromove.
6) Measure the voltage by the force sensor of the FUTEK LPM200 Panel Mount Load cell.
7) Convert the measured voltage values to the force ones.
8) Compensate the force offset to the original force values in order to obtain corrected force values. The force offset is the average of the force measured during the absence of the load, which is the deviation based on zero.
9) Filter the noise in the corrected force values to analyze the mechanical behavior of the glass fiber during the tensile testing.

In the micro-scale tensile testing, the noise is very easily triggered by the small environmental changes such as the air condition, the room temperature or the influence from external sources such as other devices near the testing setup. Thus, the low pass filter is implemented to filter the noise because there already exists the noise detected in the condition where there is no any load on the test. The procedures to build the low pass filter is described in Section 4.3.2.

4.3.2 Procedures of Filter Implementation

1) Decrease the number of the original sampling data to desired numbers by using the moving average feature by MATLAB, The MathWorks Inc. Specifically, sliding window method of the moving average is used to compute the average over the data in window. It requires setting the window length to specify the length of the sliding window and 10 is utilized as the window length in the experiment. Basic algorithm of the method is that it generates the average of the current sample and previous sample (window length -1).
2) Adjust the low pass filter until the suitable signals are obtained. In order to build the low pass filter, the window-based finite impulse response (FIR) filter is used with the frequency constraints as multi-element vector in MATLAB, The MathWorks Inc. 10 is used for the frequency constraints in the experiment.
3) Apply the low pass filter to the original sampling data to collect filtered ones.

4.3.3 Result of Open Loop System

The experiment result of the open loop system is presented in Figure 27. (a) in Figure 27 shows the measured and filtered force when sequentially increasing 0.1 mm of the displacement of the M.111.1 DG Micro-translation stage until the Jushi E6 CR glass fiber breaks. Based on the result, the grass fiber breaks when it arrives around 1.1 mm of the motor displacement from the initial position and about 0.4625 N measured force. Figure 27 (b) also represents that the force around 0.0405 N to 0.042 N is required to increase 0.1 mm motor displacement.

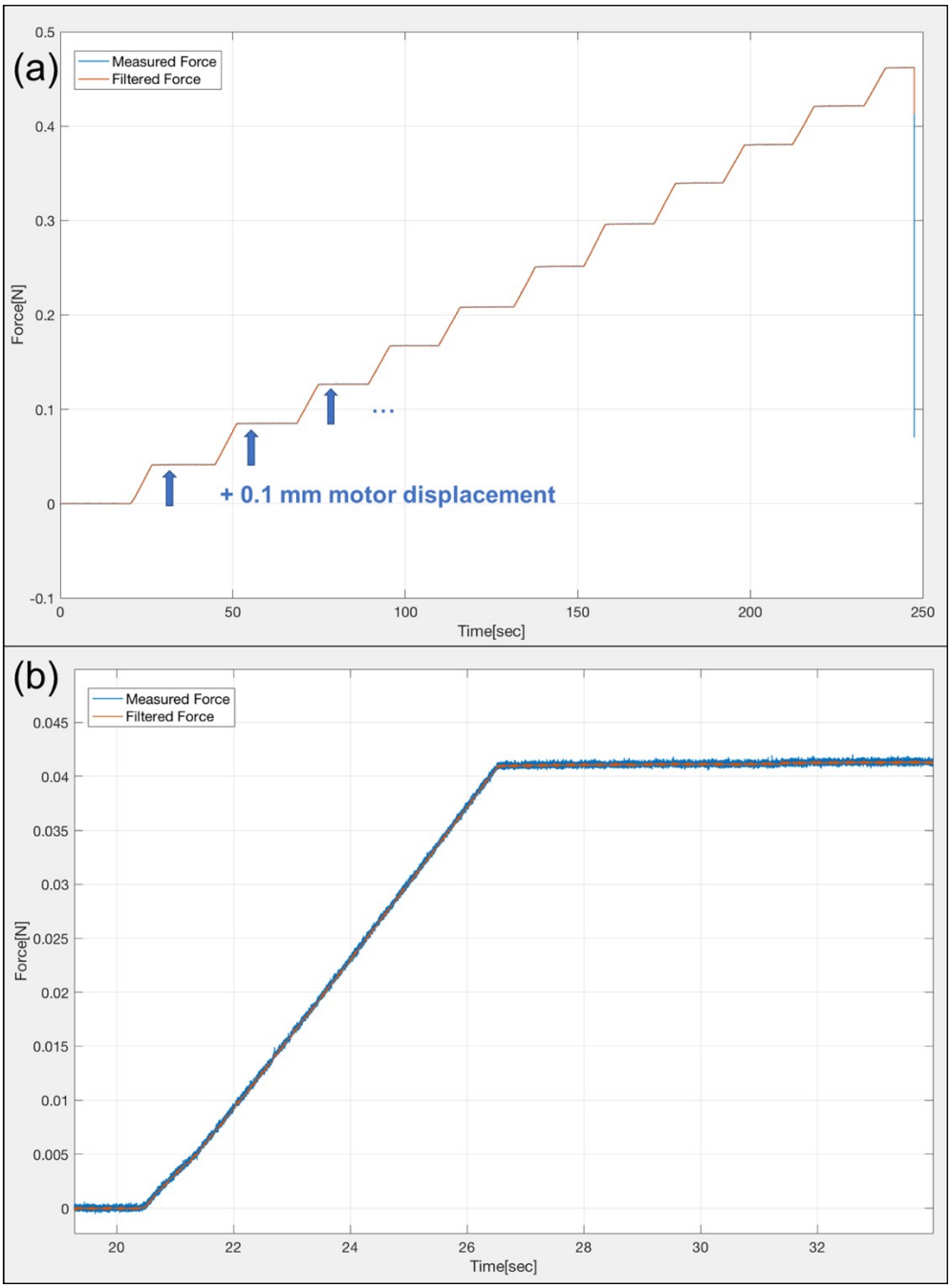

Figure 27. *Experiment result of open loop system: (a) Measured force and filtered force until the glass fiber breaks (b) Measured force and filtered force on 0.1 mm of the motor displacement*

The summary of the results by three glass fibers which are same type is shown in Table 10. Regarding the Young's modulus in Table 10, it is not possible to provide exact the Young's modulus (80 GPa) given by the manufacturer from the result of the tensile testing due to the spring constant of the load cell of the force sensor and other factors.

The Young's modulus in Table 10 is obtained by the stress and strain curve, i.e. the linear part of the curve is initially found and then, the slope is calculated to obtain the Young's modulus.

Table 10. *Summary of results for open loop system*

Fiber No.	Diame-ters	Force on break point	Motor displacement on break point	Young's Modulus
1	19.9 μm	0.4625 N (approx.)	1.1 mm (approx.)	42.58 GPa (approx.)
2	16.4 μm	0.1935 N (approx.)	0.68 mm (approx.)	42.87 GPa (approx.)
3	17.7 μm	0.32 N (approx.)	1.09 mm (approx.)	38.13 GPa (approx.)

4.4 Experiment and Result of Force Feedback Control System

For the experiment of the force feedback control system, the force feedback controller is implemented. This section describes the details of the experiment and the result. The microrobotic platform introduced in Section 4.1.1 is utilized to execute the tensile testing with the Jushi E6 CR glass fiber. Experimental procedures are described as below.

4.4.1 Experiment Procedures of Force Feedback Control System

1) Build a script to perform the force feedback control by MATLAB, MathWorks Inc. Basic algorithm of the script is shown in Figure 28 as below.

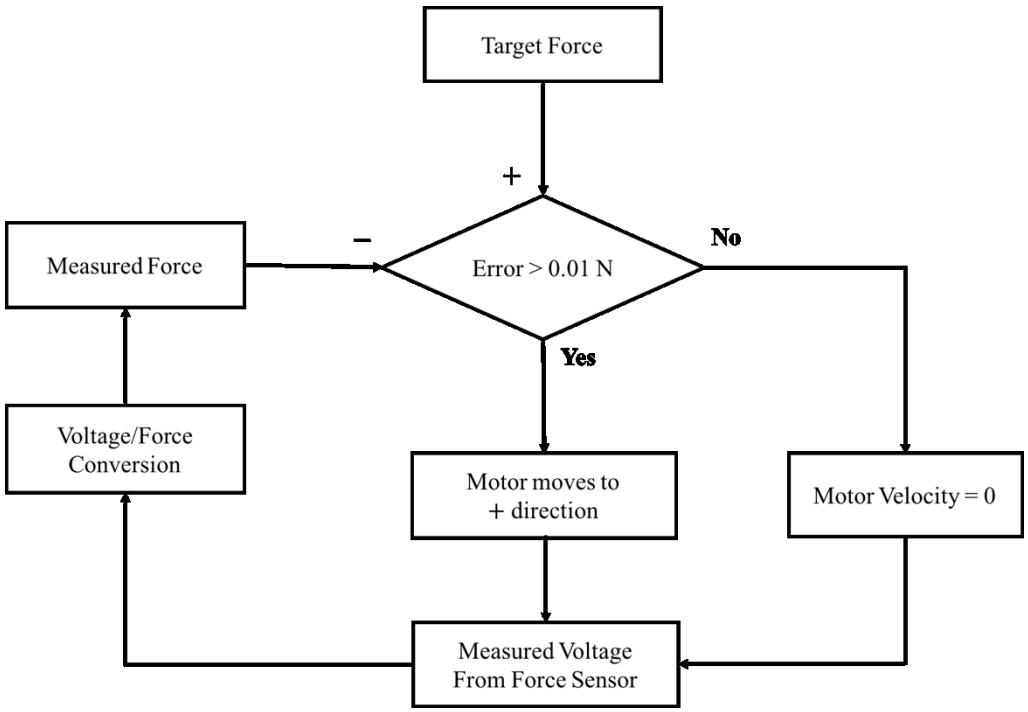

Figure 28. *Basic algorithm of force feedback controller*

2) Prepare the single Jushi E6 CR glass fiber and place it on two clamps.
3) Set 10 mm as the initial position of the M.111.1 DG Micro-translation stage and the constant velocity to 0.016 mm/s by the PImikromove.
4) Fix the glass fiber to two clamps.
5) Set the target force and the desired velocity in the script.

6) Run the script.
7) Automatically collect the measured force, error and motor position by the script

4.4.2 Result of Force Feedback Control System

The result of the force feedback controller is shown in Figure 29. Figure 29 (a) represents that the measured force approaches to the target force, 0.2 N based on the time. The red dotted line drawn on 0.19 N is the reference line, i.e. it is for showing 0.01 N reference error (error = target force $-$ measured force) described in Figure 28. As specified in Figure 28, the measured force does not reach to the target force, 0.2 N once the reference error becomes less than 0.01 N because the velocity of the DG becomes zero. The used velocity is 0.016 mm/s.

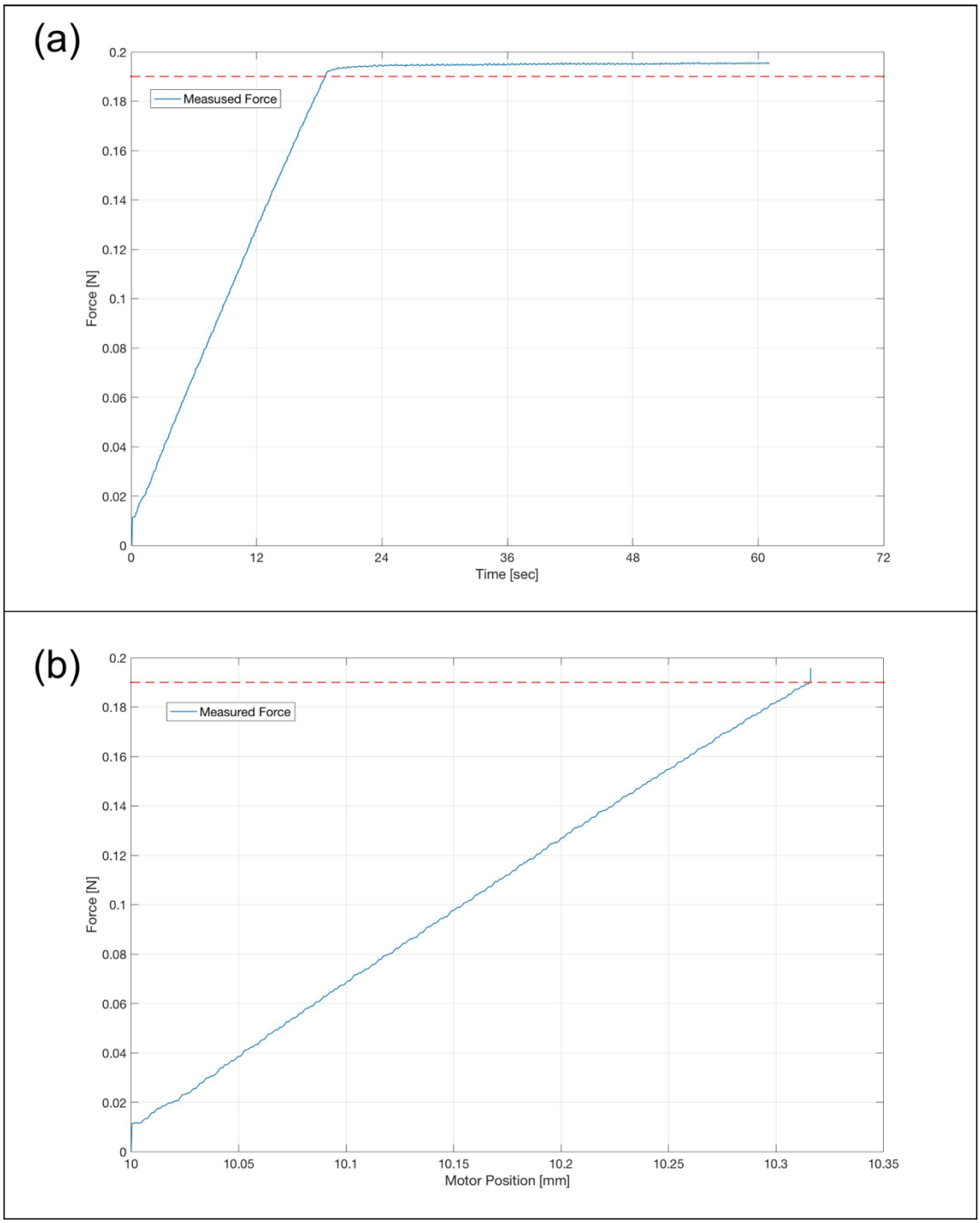

Figure 29. *Experimental result of force feedback control system: (a) Measured force based on time (b) Measured force based on motor position*

Figure 29 (b) indicates the change of the motor position depending on the measured force. Based on the result, the displacement of the motor is increased until the measured force reaches to 0.19 N due to 0.01 N reference error set in Figure 28 to make the velocity of the DG to zero. Afterward, the motor position is not changed. The measured displacement of the DG is 10.3160 mm when the error is less than 0.01 N.

Table 11 and Table 12 summarize the different behaviors of the force feedback control system depending on the different target force and velocity. Specifically, Table 11 represents the results by the different target forces, 0.2 N, 0.25 N, and 0.3 N under 0.016 mm/s constant velocity of the DG.

Table 11. *Results of force feedback control system according to different target forces under constant velocity (0.016 mm/s)*

Fiber No.	Target Force	Motor Position (< 0.01 N error)	Time (< 0.01 N error)
1	0.2 N	10.3160 mm	18.36 sec
2	0.25 N	10.7013 mm	41.13 sec
3	0.3 N	10.5131 mm	30.11 sec

Table 12 shows the results depending on the different velocity such as 0.01 mm/s, 0.016 mm/s, 0.02 mm/s, and 0.03 mm/s under 0.2 N constant target force. The results indicate the motor positions are similar even though the motor velocity is the different. It is noticeable that the spending time to enter the state that the error is less than 0.01 N is different depending on the velocity of the motor, i.e. the higher the velocity is, the shorter the spending time is.

Table 12. *Results of force feedback control system according to different velocity under constant target force (0.2 N)*

Fiber No.	Velocity	Motor Position (< 0.01 N error)	Time (< 0.01 N error)
1	0.01 mm/s	10.3270 mm	30.47 sec
2	0.016 mm/s	10.3160 mm	18.36 sec
3	0.02 mm/s	10.2810 mm	13.16 sec
4	0.03 mm/s	10.3461 mm	10.55 sec

4.5 Discussion

During the tensile test simulation by the computer model and the real experiment via the microrobotic platform, following facts are detectable as main differences between them.

1) Difference of the noise levels in the simulation and the real experiment.
2) Difficulty to implement the PID controller to the real microrobotic platform.
3) Different result mainly caused by the different mechanical property of each glass fiber.

Contrary to the computer model, there is always around $\pm 0.5\ mN$ ranges of the noise on the condition where there was no any applied load during the experiment. The reasons for the noise are various, i.e. small changes such as the air blowing from the air conditioner, room temperature and other device near the microrobotic platform can trigger such noise. In order to manage such unstable noise magnitude of the micro-scale tensile testing, either implementing suitable filter or the disturbance rejection needs to be considered in advance. However, when building the filter, the user should concern a fact that filtering too many sampling data causes inaccurate and unreliable result as it means

to lose the original data. Thus, building suitable filter is required depending on the desired level. In this thesis work, the low pass filter is utilized for the open loop system to reduce the noise as described in Section 4.3.2 and the force offset detected from the original force data is also compensated.

The initial aim for the thesis work is to implement the PID controller on the microrobotic platform. In the tensile test simulation, the PID and PI controllers are successfully employed. But in the actual experiment, due to symptom bending the glass fiber during the testing with PID controller, it is not able to successfully implement neither the PID and PI controller. The reason for the symptom may be the overshoot of the measured force triggered in the beginning of the testing. In other word, it seems that existing noise magnitude is higher than the initial pulling force measured by the force sensor. Thus, the error becomes lower than 0 which causes to move M.111.1 DG Micro-translation stage toward − direction. Therefore, the force feedback controller is implemented rather than the PID and PI controllers for the experiment. However, as the deviation between the measured force and the reference error still occurs in Figure 29, it requires improving the force feedback controller to reduce the deviation in the future.

Another difference notified is that the mechanical properties of each glass fiber such as the diameter, the Young's modulus and the stiffness can be different even though the type of the glass fibers are exactly equal. This difference causes different results of the tensile testing, which is the current problem of the existing open loop system. From the results of Table 10 in Section 4.3.3, it is noticeable that the force magnitude and the motor position of the M.111.1 DG Micro-translation stage on break point of each glass fiber are different. An obvious reason noticed is that the diameters of the glass fibers are not equal. Specifically, it is noticeable that the greater the diameter of the glass fiber is, the greater the measured force and motor displacement on break point are. The Fiber No.1 which has the largest diameter (19.9 μm) among others shows the highest measured force (0.4625 N) and motor displacement (1.1 mm) when the fiber breaks. On the other hand, The Fiber No.2 which has the smallest diameter (16.4 μm) shows exactly opposite result, i.e. the lowest measured force (0.1935 N) and motor displacement (0.68 mm) on the break point compared with those of other glass fibers. For this reason, the Young's modulus of each glass fiber measured by the results of the tensile testing is also different. The reason why the measured Young's modulus in Table 10 is different from the value provided by the manufacturer is because of the spring constant of other components in the microrobotic system, e.g. the spring constant of the force sensor and possible slippage during the measurement. However, as the measured Young's modulus of the glass fibers are similar but they are not exactly the same, it still suggests that the difference of the mechanical properties can cause the different results of the measured Young's modulus for the glass fibers and the tensile testing. Therefore, in the open loop system, it requires repeating same test with same specimen under same test method as many as possible by consuming the time in order to estimate the mechanical properties of the micro-scale fibrous materials.

In addition, the result from Table 11 in Section 4.4.2 shows the motor position and the spending time to enter the state where the error is less than 0.01 N. Based on the result of Fiber No. 2 in Table 11, the motor position, 10.7013 mm and spending time, 41.13 $\sec$ are exceptionally high compared with others although it expects that the results of Fiber No. 2 should be around between those of Fiber No. 1 and 3 in Table 11. One possible reason is also the difference of the mechanical properties of used glass fibers. Of

course, other reasons such as the structural change on the specimen by the human error during the specimen preparation has an effect on this difference.

The force feedback control can provide some benefits against aforementioned problem. For example, it offers another use case of the tensile testing. Specifically, it is useful in executing the tensile strength test by the certain target force applied to the glass fiber or other micro-scale fibrous materials as it controls the pulling force to reach to the target force no matter whether the mechanical properties of the specimen are different or not as shown in Table 11. Also, the force feedback control can compensate to a certain extent against the noise, even though it still needs to consider the proper strategy of the noise rejection to resolve the aforementioned symptom with the PID controller.

5 CONCLUSION

In this thesis work, the force feedback controller is implemented and applied to the microrobotic platform. By doing so, it is able to control the tensile force of the micro-scale fibrous materials such as the glass fiber relying on the applied target force. It is meaningful thesis work as it is a first trial to apply the force feedback control to the application of the micro-scale fibrous material testing. Table 13 sums up key parts of the thesis work.

Table 13. *Summary of key points of the thesis work*

Objective	• Implement the force feedback controller of the exiting microrobotic platform used in the micro-scale fibrous material testing.
Procedure	1) Understand the theoretical background on the force control and the tensile testing, including general method and applications in micro- and nano scale. 2) Build the mathematical model based on specified parameters of the M-111.1 DG Micro-translation stage and the glass fibers. 3) Build the computer model based on the mathematical model by the PID and PI controllers via the Simulink, The MathWorks Inc. The computer model includes nonlinear elements such as the dead zone, the backlash, and the friction to increase the disturbance. 4) Tune the PI and PID controller parameters by the conventional rule based tuning methods such as the Ziegler Nichols [47][48], the PIAE [48], SO-OV [48],and NO-OV [48], and the Simulink PID tuner [49]. 5) Simulate the tensile testing by the computer model. 6) Understand the behavior and the limitation of the existing open-loop microrobotic platform by performing the actual experiment. 7) Understand the influence of fiber properties on open loop force control 8) Implement the force feedback controller by MATLAB, The MathWorks Inc.

	9) Perform the tensile test under the specified target force to control the measured force when the clamp pulls the Jushi E6 CR glass fiber on the microrobotic platform.
Result	• The computer model of the microrobotic platform is successfully implemented and simulated for the micro-tensile testing. • The force feedback controller is successfully implemented and applied to the existing microrobotic platform. • The force feedback controller controls the pulling force depending on the input target force. The pulling force is measured by the force sensor when the glass fiber is pulled by the clamp.
Findings	1) In the simulation of the computer model, the controller parameters tuned by the NO-OV is the most reasonable in this material testing application because it results in the lowest overshoot ($\pm$ 1 %) of the output signals against different types of input signals, which can prevent the micro-scale fibrous materials from breaking during the tensile testing. 2) Big difference of the noise levels between the simulation and actual experiment is detected. In the real experiment, $\pm$ 0.5 mN ranges of the noise always exists when there is no load to the glass fiber. For this reason, the low pass filter is implemented and applied to the open loop microrobotic platform in order to filter the massive noise. 3) The difference of the mechanical properties of each glass fiber generates inaccurate and unreliable result in the end. As noticed in Table 10, although all glass fibers used are same type, i.e. Jushi E6 CR glass fiber, the diameters of each glass fiber are different. Then, this difference generates different results of the position of the DG and measured force on break point of the glass fiber. Specifically, the greater the diameter of the glass fiber is, the greater the measured force and the DG positon are when the glass fiber breaks, and vice versa. For this reason, the calculated Young's modulus of the glass fibers is also different. 4) The force feedback controller controls the input target force no matter whether the mechanical properties of the glass fibers is equal or not. Thus, it can be used in executing the tensile strength test under the certain target force applied to the micro-scale fibrous materials.

Difficulty	• It is difficult to control the movement of the M-111.1 DG Micro-translation stage during the overshoot when using PID controller. Due to the reason, the symptom bending glass fiber occurs, i.e. the M-111.1 DG Micro-translation stage move to - direction, even though it should move to + direction when the clamp starts pulling the glass fiber to reach to the target force. One of the reasons seems to be the low force magnitude in the beginning of the testing which are below normal noise level measured. Thus, the error becomes lower than 0 which causes to move M.111.1 DG Micro-translation stage toward −direction.
Future work	1) Implement an improved controller to reduce the deviation between the measured force and the reference error. 2) Resolve the symptom where the M-111.1 DG Micro-translation stage moves to - direction at the beginning of the test execution. For this, it requires suitable noise rejection and work to improve the control algorithm. 3) Add the velocity control in the force feedback controller so that microrobotic platform is able to control the velocity of the DG in the M-111.1 DG Micro-translation stage depending on the error magnitude.

Eventually, the RQ3 stated in Section 1.2 is answered in following.

RQ1. How can the force feedback control be applied to the microrobotic platform designed for the micro-tensile testing of the micro-scale fibrous materials?

As none of the studies have tried to apply the force feedback control to the microrobotic platform for the micro-tensile testing of the micro fibrous materials, the novel way was introduced in Chapter 3 and 4 of the thesis. First, the mathematical models of the microrobotic platform with the glass fiber were explained. Second, the author built the computer model for the tensile testing simulation by using the mathematical models and tuned controller parameters by the different tuning methods to obtain the usable ones. Finally, the force feedback control was successfully implemented to the real microrobotic platform to control the pulling force depending on the reference error between the target input force and the measured force.

REFERENCES

[1] L. Villani, L, J. De Schutter, Force Control, Springer Handbook of Robotics, 2008, 161-185 p. DOI: 10.1152/japplphysiol.00462.2011

[2] L. Antoio, F. Almeida, A force–impedance controlled industrial robot using an active robotic auxiliary device, Robotics and Computer-Integrated Manufacturing, 2008. DOI: 10.1016/j.rcim.2007.04.002

[3] T. Winiarski, A, Wozniak, Indirect force control development procedure, Cambridge University Press 2012, 465-478 p. DOI: 10.1017/S0263574712000446

[4] J. Ahn, S. Lee, S. Jung, Force control application to a mobile manipulator with balancing mechanism, IECON 2010 - 36th Annual Conference on IEEE Industrial Electronics Society, 2010, 1528-1533 p. DOI: 10.1109/IECON.2010.5675455

[5] J. Pires, T. Godinho, R. Araújo, Force control for industrial applications using a fuzzy PI controller, Sensor Review, 2004, 60-67 p. DOI: 10.1108/02602280410515833

[6] N. Hogan, Impedance control: An approach to manipulation, American Control Conference, 1984, 304-313 p.

[7] A. Busu, M. Shamil Jaffarullah, C. Yee Low, et al. A Review of Force Control Techniques in Friction Stir Process, Procedia Computer Science, 2015, 528-533 p. Available: www.sciencedirect.com

[8] M. C. Carrozza, A. Eisinberg, A. Menchiassi et al. Towards a force-controlled microgripper for assembling biomedical microdevices, Journal of Micromechanics and Microengineering Volume 10, Number 2, 2000, 271-276 p.

[9] A. Esinberg, A. Menciassi, S. Micera et al. PI force control of a microgripper for assembling biomedical microdevices, IEEE Proceedings-Circuits Devices and Systems, 2001, 348-352 p. DOI: 10.1049/ip-cds:20010172

[10] Y. Zhou, B. J. Nelson, The effect of material properties and gripping force on micrograsping, IEEE International Conference on Robotics and Automation, 2000, 1115-1120 p. DOI: 10.1109/ROBOT.2000.844748

[11] D. H. Kim, B. Kim, H. Kang et al, Development of a piezoelectric polymer-based sensorized microgripper for microassembly and micromanipulation, IEEE International Conference on Intelligent Robots and Systems, 2004, 275-280 p. DOI: 10.1007/s00542-003-0330-y

[12] J. Park, S. Kim. D. H. Kim et al, Identification and Control of a Sensorized Microgripper for Micromanipulation, IEEE/ASME Transactions on Mechatronics, 2005, 601-606 p. DOI: 10.1109/TMECH.2005.856103

[13] M. Tomizuka, Zero phase error tracking algorithm for digital control, Journal of Dynamic Systems Measurement and Control, 1987, 65-68 p. DOI: 10.1115/1.3143822

[14] K. Kim, X. Liu, Y. Zhang et al, MicroNewton force-controlled manipulation of biomaterials using a monolithic MEMS microgripper with two-axis force feedback, IEEE International Conference on Robotics and Automation, 2008, 3100-3105 p. DOI: 10.1109/ROBOT.2008.4543682

[15] X. Liu, K. Kim, Y. Zhang et al, NanoNewton force sensing and control in microrobotic cell manipulation, International Journal of Robotics Research, 2009, 1065-1076 p. DOI: 10.1177/0278364909340212

[16] M. Boudaoud, S. Regnier, An overview on gripping force measurement at the micro and nano-scales using two-fingered microrobotic systems, International Journal of Advanced Robotic Systems, 2014. DOI: 10.5772/57571

[17] H. Ghafarirad, S. Rezaei, A. Sarhan et al. Modified robust external force control with disturbance rejection with application to piezoelectric actuators, Transactions of the Institute of Measurement and Control, 2015, 131-143 p. DOI: 10.1177/0142331214535409

[18] E. Tan, C. Lim, Novel approach to tensile testing of micro- and nanoscale fibers, Review of Scientific Instruments, 2004, 2581-2585 p. DOI: 10.1063/1.1775309

[19] X. Nie, B. Song, Y.Ge et al, Dynamic Tensile Testing of Soft Materials, Experimental Mechanics, 2009, 451-458 p. DOI: 10.1007/s11340-008-9133-5

[20] P. Wang, X. Zhang, R. Hansen et al. Strengthening and failure mechanisms of individual carbon nanotube fibers under dynamic tensile loading, Carbon, 2016, 18-31 p. DOI: 10.1016/j.carbon.2016.02.009

[21] P. Saketi, Microrobotic platform with integrated force sensing microgrippers for characterization of fibrous materials : Case study on individual paper fibers, Tampere University of Technology, 2016, ISBN: 9789521535451

[22] F. Hosseinali, Investigation on the Tensile properties of Individual Cotton Fibers, Texas Tech University, 2012

[23] P. Saketi, A. Treimanis, P. Pedro et al, Microrobotic platform for manipulation and flexibility measurement of individual paper fibers, CEUR Workshop Proceedings, 2015, 33-36 p. DOI: 10.1017/CBO9781107415324.004

[24] P. Saketi, M. von Essen, M. Mikczinski et al, A flexible microrobotic platform for handling microscale specimens of fibrous materials for microscopic studies, Journal of Microscopy, 2012, 163-171 p. DOI: http://dx.doi.org/10.1111/j.1365-2818.2012.03660.x

[25] W. Sharpe, K. Turner, R. Edwards, Tensile testing of polysilicon, Experimental Mechanics, 1999, 162-170 p. DOI: 10.1007/BF02323548

[26] M. Haque, M. Saif, Application of MEMS force sensors for in situ mechanical characterization of nano-scale thin films in SEM and TEM, Sensors and Actuators, A: Physical, 2002, 239-245 p. DOI: 10.1016/S0924-4247(01)00861-5

[27] M. Haque, M. Saif, Mechanical behavior of 30-50 nm thick aluminum films under uniaxial tension, Scripta Materialia, 2002, 863-867 p. DOI: 10.1016/S1359-6462(02)00306-8

[28] E. Bamberg, C. Grippo. P. Wanakamol et al, A tensile test device for in situ atomic force microscope mechanical testing, Precision Engineering, 2006, 71-84 p. DOI: 10.1016/j.precisioneng.2005.05.001

[29] W. Sharpe Jr, Technical Interferometric Strain / Displacement, NASA Technical Memorandum, 1989.

[30] W. Sharpe, B. Yuan, R. Edwards, A new technique for measuring the mechanical properties of thin films, Journal of Microelectromechanical Systems, 1997, 193-199 p. Available: http://ieeexplore.ieee.org/lpdocs/epic03/wrapper.htm?arnumber=623107

[31] M. Zupan, M. Hayden, C. Boehlert et al, Development of High-temperature Microsample Testing, Experiment mechanics, 2001, 242-247 p. DOI: 10.1007/BF02323140

[32] M. Cheng, W. Chen, T. Weerasooriya, Mechanical Properties of Kevlar® KM2 Single Fiber, Journal of Engineering Materials and Technology, 2005, 197-203 p. DOI: 10.1115/1.1857937

[33] J. Lim, J.Q. Zheng, K. Masters et al, Mechanical behavior of A265 single fibers, Journal of Materials Science, 2010, 652-661 p. DOI: 10.1007/s10853-009-3979-5

[34] J. Lim, W. Chen, J.Q. Zheng, Dynamic small strain measurements of Kevlar® 129 single fibers with a miniaturized tension Kolsky bar, Polymer Testing, 2010, 701-705 p. Available: http://dx.doi.org/10.1016/j.polymertesting.2010.05.012

[35] W. Liu, K. Bonin, M. Guthold, Easy and direct method for calibrating atomic force microscopy lateral force measurements, Review of Scientific Instruments, 2007, DOI: 10.1063/1.2745733

[36] A. Gestos, P. Whitten, G. Spinks et al, Tensile testing of individual glassy, rubbery and hydrogel electrospun polymer nanofibers to high strain using the atomic force microscope, Polymer Testing, 2013, 655-664 p. Available: http://dx.doi.org/10.1016/j.polymertesting.2013.02.010

[37] T. Tsuchiya, M. Shikida, K. Sato, Tensile testing system for sub-micrometer thick films, Sensors and Actuators, A: Physical, 2002, 492-496 p. DOI: 10.1016/S0924-4247(01)00862-7

[38] Y. Cheng, D. Read, J. McColskey et al, A tensile-testing technique for micrometer-sized free-standing thin films, Thin Solid Films, 2005, 426-432 p. DOI: 10.1016/j.tsf.2005.03.030

[39] Y. Zhu, H. Espinosa, An electromechanical material testing system for in situ electron microscopy and applications, Proceedings of the National Academy of Sciences of the United States of America, 2005, 4503–14508 p. Available: http://www.pnas.org/content/102/41/14503.abstract

[40] U. Lang, M. Reichen, J. Dual, Fabrication of a tensile test for polymer micromechanics, Microelectronic Engineering, 2006, 1182-1184 p. DOI: 10.1016/j.mee.2006.01.050

[41] K. Nagayama, S. Yanagihara, T. Matsumoto, A novel micro tensile tester with feed-back control for viscoelastic analysis of single isolated smooth muscle cells, Medical engineering and physics, 2007, 620-628 p. DOI: 10.1016/j.medengphy.2006.08.003

[42] Physik Instrumente (PI) GmbH & Co., M-11x Micro-translation stage User Manual, Available: https://www.physikinstrumente.com/

[43] Physik Instrumente (PI) GmbH & Co., C-863 Mercury DC Motor Controller User Manual, Available: https://www.physikinstrumente.com/

[44] F. Szufnarowski, A. Schneider, W. Federle, Development of a force feedback and measurement system for the analysis of the biomechanics of insect attachment organs, University of Bielefeld, 2008.

[45] FUTEK Advanced Sensor Technology Inc., LPM200 Panel Mount Load Cell Spec sheet, Available: http://www.futek.com/files/pdf/Product%20Drawings/FSH03398.pdf

[46] Physik Instrumente (PI) GmbH & Co., M-11x Micro-translation stage User Manual, Available: https://www.physikinstrumente.com/

[47] J. Ziegler, N. Nichols, Optimum settings for automatic controllers, InTech, 1995, 94-100 p. DOI: 10.1115/1.2899060

[48] A. McCormack, K. Godfrey, Rule-based autotuning based on frequency domain identification, Control Systems Technology, 1998, 43-61 p. DOI: 10.1109/87.654876

[49] The MathWorks Inc., Natick, MA, Simulink Documentation, Available: https://se.mathworks.com/help/slcontrol/gs/automated-tuning-of-simulink-pid-controller-block.html